

# BIOMASS CONVERSION TO FUELS AND CHEMICALS

Helena L. Chum and Ralph P. Overend

National Bioenergy Center  
National Renewable Energy Laboratory  
1617 Cole Boulevard, Golden, Colorado, USA

## Introduction

Biomass has a significant potential to provide liquid, solid and gaseous fuels in conjunction with the co-production of food, feed, fiber and new bioproducts. The selection of a conversion technology will be a function of both the supply of locally available feedstock and the markets for products and will determine the degree to which various biological and chemical routes are deployed. This paper reviews the major technical principles and challenges in the evaluation of feedstocks and conversion systems for the energy markets of the future. The challenges of energy supply, reliability, environmental performance and lifecycle impacts will also be discussed for thermochemical biomass conversion via gasification.

## Biomass Supply

The growing acceptance of biomass as the only renewable source of carbon for the future requires that a realistic appraisal of its potential be undertaken. While solar energy captured by wind, PV or high temperature concentrating solar systems, have very high energy supply potentials—far exceeding today's total primary energy supply of approximately 417 EJ (IEA, TPES data for 2000)—it will be delivered in the form of electricity and potentially hydrogen. However, before a purely hydrogen and electrical economy can arrive, during the 21<sup>st</sup> century the world has to undergo a carbon usage transition from directly emitting fossil carbon dioxide into the atmosphere to one in which fossil carbon is captured and sequestered, and biomass becomes the sole form of the earth's carbon resource that can be emitted directly to the atmosphere due to its short term photosynthetic cycle in the biosphere.

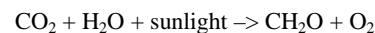
Unlike fossil fuels for which exploration, discovery and assessment of resources and reserves is a well known science, renewable energy accounting introduces a flow concept to describe the size and availability of the resource. Biomass is rather unusual; it exists somewhere between the intermittent, flux-only resources such as solar and wind, and the traditional fossil fuel stock perspective. This is because of its annual and perennial storage capability, allowing dispersed and captured solar energy to be concentrated and converted into useful, energy and products on a continuous basis at centralized facilities according to normal demand patterns. Thus, the photosynthesis process of solar collection, crop harvest, and transport of biomass fuels will define the availability of biomass for energy and materials purposes.

As with fossil resources, the energy conversion technologies play a huge role in enabling the solar resources by dictating the efficiency, and the utility of renewables with respect to society and the environment—in sum, their sustainability. However, this presentation will concentrate on the biomass system only up to the conversion plant gate.

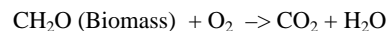
## Biomass resources in the USA

The renewable energy cycle for biomass starts with photosynthesis, which captures the fraction of light between 400 nm and 700 nm in the solar spectrum to provide the energy to fix carbon

dioxide and split water molecules, producing raw photosynthate according to the equation:



The photosynthate formula, CH<sub>2</sub>O, is essentially the same as sugar, starch, or cellulose, the latter being the most common natural polymer on earth. Energy is obtained from biomass by means of combustion with oxygen as in a fire, or through metabolic processes, e.g., respiration to provide chemical energy for muscles and other processes:



Either way, the net result is a closed cycle in which carbon dioxide and water vapor are returned to the atmosphere. This solar-energy powered closed-loop supports all life on earth, providing food for humanity, feed for animals, fibers for clothing, and materials for buildings and consumer products, in addition to fuel.

A theoretical estimate of the efficiency of photosynthesis is about 5.5%. The energy received from the sun at any given location varies with latitude and season; and the annual photosynthetic capture is a function of the water and nutrient availability and the seasonal climate variations. As a result actual crops achieve much less than this. The variation is very large ranging from the annual accumulation of less than 1 t ha<sup>-1</sup> y<sup>-1</sup> of dry biomass in a mature boreal forest, to approximately 50 t ha<sup>-1</sup> y<sup>-1</sup> of total biomass for a record corn yield (in Iowa, in 1999) of 408.2 bushels of corn per acre. This is calculated by accounting for the stalk and other above ground biomass components by means of the harvest index, which has a value of 0.5 applied to the 25.6 t ha<sup>-1</sup> y<sup>-1</sup> of corn kernels.

## Sources of bioenergy

The primary biomass sources are natural forests, planted trees and shrubs, and agricultural crops. However, much of today's bioenergy is derived from secondary, tertiary, and post-consumer residues derived from these primary resources. Secondary residues are mainly harvesting residues and include: forest slash; crop residues such as straw and stover from cereal production; as well as minor sources such as orchard, rights of way, and vineyard prunings. Tertiary sources are usually process residues and include: black liquor produced in kraft pulping; sawdust and bark from solid wood processing; and sugar cane bagasse. Food processing tertiary residues include: orange and potato peelings; and large quantities of water containing various amounts of proteins, starches, and sugars. Animal operations that produce dairy products, eggs, and meat generate a large stream of residues (at ever increasing scales) from large feedlot operations. These are becoming regulated as concentrated animal feed operations (CAFO)s. These tertiary residues are usually high moisture and most often are treated by a process of anaerobic digestion to produce biogas, a mixture of methane and carbon dioxide, as fuel.

Much of the post consumer residues are in fact biomass: paper, packaging, crates, pallets, demolition lumber, food scraps, and sewage treatment residues. These are more and more often entering the bioenergy, biofuels, and bioproducts stream as society practices resource conservation and use. The Environmental Protection Agency's (EPA) preferred method is source reduction, which includes reuse, followed by recycling and composting, and, lastly, disposal in combustion facilities and landfills.

These primary, secondary, tertiary, and post consumer pathways are significant when compared with the US TPES of about 100 EJ. The total forest harvest is on the order of 203 M tonnes of air-dried

round wood equivalents per year, which corresponds to > 3.5 EJ of primary energy equivalent. In recent years the annual corn harvest of almost 10 billion bushels (254 Mt) corresponds to over 4 EJ of primary energy equivalent produced on 3,000 km<sup>2</sup> (about 75 million acres, or about half of the arable crop area of the USA). Though corn stover is partly required to remain on the land to maintain fertility and reduce soil erosion, the quantity available is similar to the amount of crop and represents the largest agricultural residue potential.

### **Effect of Transportation on Cost**

The key determinant of the feasibility of biomass is the cost of the biomass that contains the stored “free” solar energy. As the cost varies with the transportation distance from the process plant to the field or forest, as well as the opportunity cost of the feedstock, the cost is usually obtained from a supply curve. There are many factors that go into deriving the supply curve for the resource. Due to the bulk of biomass, its transportation over long distances by road is not economical, though with low cost transportation by rail, the distance can be increased. While an 80 km collection is often cited, this is only an order of magnitude. In each case, the actual collection radius will be a function of the biomass density per unit area, the nature of the terrain, road network density, and the condition and type of transportation available.

### **Density Relationship**

One of the highest biomass densities is, in fact, the post consumer residue production of the urban areas. Cities draw upon the resources of vast areas and concentrate them in a small area resulting in a “footprint” that is much greater than the physical urban area. A useful number is a *per capita* urban residue energy generation rate of about 22 MJ *caput*<sup>-1</sup> d<sup>-1</sup> (1.86 kg d<sup>-1</sup> of residue with 11.6 MJ kg<sup>-1</sup> heat of combustion, 1990). Major metropolitan areas have population densities of greater than 2000 person km<sup>-2</sup>. For this population density, the thermal energy equivalent in their residues is about 4.4 GWh km<sup>-2</sup>. If a short rotation woody crop was grown at yields of 15 tonne ha<sup>-1</sup> y<sup>-1</sup>, it would produce about 7.8 GWh km<sup>-2</sup>.

### **Conclusion**

The predicted 2020 potential of biomass costing less than 4 \$ GJ<sup>-1</sup> is about 8 EJ. The sources and constraints on the biomass resources contributing to this total will be discussed.

# BIO-OIL FROM RICE STRAW BY PYROLYSIS USING FLUIDIZED BED AND CHAR REMOVAL SYSTEM

Young-Kwon Park<sup>1</sup>, Jong-Ki Jeon<sup>2</sup>, Seungdo Kim<sup>3</sup>,  
Joo-Sik Kim<sup>1\*</sup>

(1) Faculty of Environ. Eng. Univ. of Seoul, Seoul, Korea  
(2) Dept. of Chem. Eng., Dongyang Univ., Youngjou, Korea  
(3) Dept. of Environ. System Eng., Hallym Univ. Chuncheon, Korea  
\* Corresponding author: [joojik@uos.ac.kr](mailto:joojik@uos.ac.kr)

## Introduction

Rice straw is one of abundant biomass whose production sums up to about 7 million ton annually in Korea. It is usually utilized as a compost or forage in Korea. Nowadays intensive attention has been paid to rice straw from the viewpoint of a potential renewable energy source, due to high price of petroleum. Thermochemical conversion of biomass is one of the most common routes for conversion into energy. Among thermochemical conversion processes, pyrolysis of biomass is a promising tool to provide bio-oil which can be used as an alternative fuel oil or chemical feedstocks. In the last two decades, extensive researches have been carried out to understand the complexity of pyrolysis, to obtain optimal conditions for producing bio-oil, and to analyze the composition of bio-oil quantitatively and qualitatively. A great portion of past researches have focused on the pyrolysis of wood or wood wastes. Pyrolysis of rice straw, however, has been conducted not so intensively and once it is performed, only in small laboratory scale plants. This paper reports the results of pyrolysis of rice straw in a bench scale plant equipped mainly with a fluidized bed, a char separating system and a quench system. We investigated the influence of reaction temperature on the production of bio-oil, the efficiency of a char-separating system and some physical and chemical analyses of bio-oil, product gas and char.

## Experimental

**Rice straw.** Rice straw obtained from a province in Korea was cut into rectangular form with a size of about 5 mm. Including elemental analysis, some analyses were performed. Table 1 shows characteristics of rice straw fed. The amount of cellulose, hemicellulose and lignin is based on volatile portion of rice straw.

Table 1. Analysis of rice straw.

Composition	wt%
cellulose	54.67
hemicellulose	32.53
lignin	12.83
Water, ash, volatile	wt%
water	6.48
volatile	82.30
ash	11.22
Elemental analysis	wt%
C	39.2
H	4.84
N	1.60
S	0.67
O	53.69
Alkali metal	Concentration (ppm)
Na	250
Mg	930
Ca	2100
K	12000

**Bench scale pyrolysis plant.** Experiments were carried out using a bench scale plant with a capacity of up to 3 kg/h. The fluidized bed reactor made of sus-304 has a free diameter of 154mm and a length of 616 mm. It is heated indirectly by electric power. Rice straw enters the reactor through two screw conveyors and then is pyrolyzed. A cyclone and a hot filter serve as char separator. These separators are heated up to 400 °C to prevent from the condensation of product gas. A series of quenching system is applied to cool product gas efficiently and quickly. Product gas is circulated into the fluidized bed using a compressor.

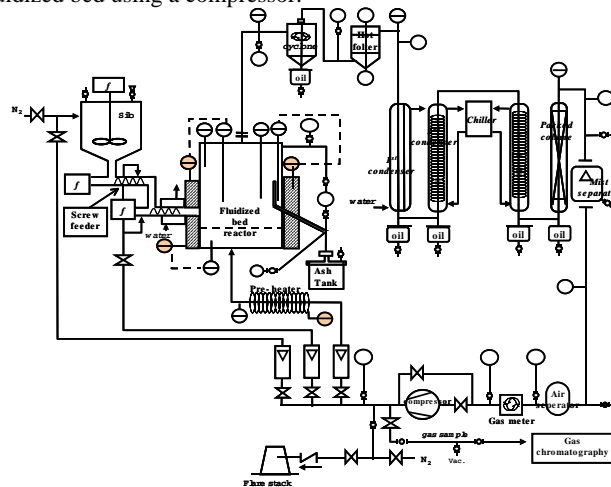


Figure 1. Fluidized bed reactor system.

**Reaction conditions.** Reaction conditions are shown in Table 2. In every experiment, particle size of feed was about 5 mm and product gas was served as a fluidizing medium. The residence time of product gas in the reactor lay ca. 2 or 3 seconds in each experiment and this makes it possible to compare the influence of reaction temperature on the product spectrum relatively clearly. Particle size of the sand used in the fluidized bed was ca. 0.4 mm.

Table 2. Parameters of experiments.

	Run1	Run2	Run3	Run4	Run5
Temperature (°C)	412	443	516	545	598
Amount of input (g)	1700	1500	1560	1500	1500
Duration (min)	118	87	67	80	80
Feed rate (g/h)	864	1034	1397	1125	1125

**Analysis.** Qualitative and quantitative analysis of pyrolysis gas and oil has been performed by GC and GC-MS system. Using ICP the content of alkali metals in products was also analyzed. Solid content in bio-oil was measured using acetone as a solvent. In addition to chemical analysis, physical characteristics of bio-oil was also examined, such as density, viscosity etc.

## Results and Discussion

**Mass balance** The behavior of biomass pyrolysis is dependent on many parameters, such as reaction temperature, residence time of gas in reactor, particle size of feed material and feed rate. This paper focuses on the influence of reaction temperature. Mass balance of each experiment is shown in Figure 2. As reaction temperature rises, the amount of gas increases. It is also shown that there is an optimum temperature to produce more bio-oil. In the reaction temperature range between 412 and 516 °C, the yield of oil was relative constant to give a maximum yield of 50 wt% and then decreases distinctly with increasing temperature.

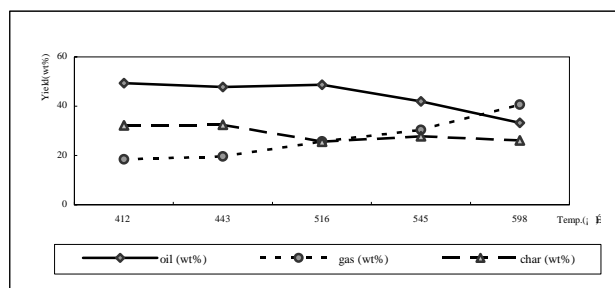


Figure 2. Product distribution with temperature.

This tendency is typical for the pyrolysis of biomass, which results from the secondary reaction of volatiles[1]. The yield of bio-oil is lower than in the case of pyrolysis of wood, which is largely due to lower content of organic portion in rice straw than in wood and a larger content of ash in rice straw, some metallic components in which lower the yield of bio-oil by catalytic decomposition of oil portion. The use of hot filter can reduce the yield of bio-oil in which thermal cracking of pyrolysis vapor takes place. In the experiments, we used rice straw particle whose diameter lies about 5 mm for easy transporting it into the reactor. This relative larger size in comparison with typical pyrolysis of biomass can have an influence on the reduction of bio-oil yield [2].

**Product gas.** Figure 3 shows the development of main components in product gas with temperature. Methane, CO and CO<sub>2</sub> consist mainly of product gas. Ethene and ethane was other important components in the product gas. Hydrogen content was under 1 wt% in every experiment. It is shown in the Figure 3 that higher temperature leads to high yield of methane and CO, which results mainly from the secondary cracking of volatiles[3]. This tendency including higher content of other hydrocarbon gases at elevated reaction temperature gives high heating value to product gas.

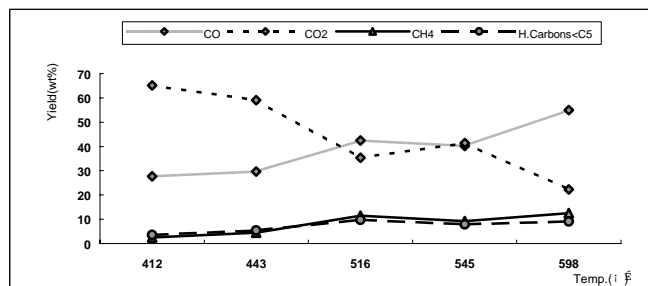


Figure 3. Gas composition with temperature

**Bio-oil.** Obtained bio-oil shows a phase separation. Large portion of tar was deposited in bio-oil containers. Therefore, it was very difficult to sample it accurately. We conducted sampling according to the procedure at VTT and various chemical and physical characterizations of bio-oil were carried out [4]. Some distinct features of bio-oil are listed in Table 3. Water content in bio-oil was very variable according to samples but lay in the range of 50-60wt%. Product oil showed nearly metal-free character, which simplifies the treatment of bio-oil during up-grading and reduces catalytic reactions during storage. Reduction of density and increase of pH value in comparison with typical bio-oil from wood is caused mainly by high content of water in bio-oil. Solid content in bio-oil lay around 0.03 wt%. The value is somewhat high in comparison with mineral oil whose value is about 0.01 wt%. Applying of a hot filter, however, reduced solid content distinctly, compared with other processes

without it. Solid seems to consist of hydrocarbons implied by the ash content in bio-oil (0.007 wt%).

Table 3. Characteristics of bio-oil.

Analysis		Run5 (598 °C)
Alkali Metals (g/L)	Na	not detected
	Ca	4
	Mg	under 1
	K	3
Solid content (wt%)		0.03
pH		4.07
Ash (wt%)		0.007
Density (15 °C, g/cm <sup>3</sup> )		1.0089
Flash point (°C)		69
Pour point (°C)		-10
Viscosity (50 °C, cSt)		71

Bio-oil was analyzed by GC and GC-MS system. Using acetone as a solvent, qualitative analysis was conducted. Some typical components, such as acetic acid, phenol and alkylated phenols, furan derivatives, furfural and anhydrosugers were identified.

**Char.** Char formed during pyrolysis serves as vapor cracking catalysts to reduce the yield of bio-oil. It can also raise bio-oil viscosity through catalytic reaction during storage, and is likely to be detrimental to most applications. Therefore efficient removal of char is necessary for the production of bio-oil of high quality. We used a hot filter and a cyclone for removal of char. In cyclone, particles with sizes of 10-100 μm were captured. In contrast, the hot filter could catch particle size around 0.1μm. Most of alkali metals in feed was found in char and the C/H ratio of char was in the range of 4 and 5. Figure 4 shows the particle size distributions of char obtained in hot filter.

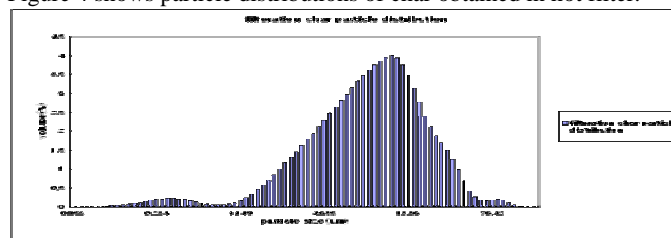


Figure 4. Particle size distribution of char from hot filter.

## Conclusion

High quality bio-oil was obtained from rice straw using a fluidized reactor and a char removal system. Optimum reaction temperature for the high yield of bio-oil lay between 410 and 510 °C. Bio-oils obtained in experiments showed very low content of alkali metals, and solid content in bio-oil was about 0.03wt%. In the future, some more works are needed for more yield of bio-oil with smaller size of particle to feed and less water content in feed by drying.

**Acknowledgment.** This subject is supported by the Ministry of Environment in Korea as "The Eco-technopia 21 project".

## References

1. Bradbury, A.G.W., Sakai, Y. and Shafizadeh, F., J. Appl. Polym. Sci., 1979, Vol. 23, pp. 3271.
2. Dobele, G. in Bridgwater, et al., Fast Pyrolysis of Biomass: Handbook Vol. 2, pp150, CPL Press: Newbury, 2002.
3. Radlein, D., in Bridgwater et al., Fast Pyrolysis of Biomass: A Handbook, pp165, CPL Press: Newbury, 1999.
4. Oasmaa, A., et al, Physical characterisation of biomass-based pyrolysis liquids, VTT Publication 306, pp12, Espoo, 1997

## VALUABLE AND STABLE CARBON CO-PRODUCT FROM FOSSIL FUEL EXHAUST SCRUBBING

Danny Day <sup>\*1</sup>, Robert J. Evans<sup>2</sup>, James W. Lee<sup>3</sup>, Don Reicosky<sup>4</sup>

<sup>1</sup>Eprida, Inc., 6300 Powers Ferry Road, Suite 307, Atlanta, GA 30339  
[danny.day@eprida.com](mailto:danny.day@eprida.com)

<sup>2</sup>National Renewable Energy Laboratory, 1617 Cole Blvd, Golden, CO, 80401, [bob\\_evans@nrel.gov](mailto:bob_evans@nrel.gov)

<sup>3</sup>Oak Ridge National Laboratory, 4500N, A16, MS-6194, Oak Ridge, TN 37831, [leejw@ornl.gov](mailto:leejw@ornl.gov)

<sup>4</sup>USDA-Agricultural Research Service, 803 Iowa Avenue, Morris, MN 56267 [reicosky@morris.ars.usda.gov](mailto:reicosky@morris.ars.usda.gov)

### Introduction

**A Sustainable Carbon Sink With Hydrogen Production.** The increasing anthropogenic CO<sub>2</sub> emissions and possible global warming have challenged the United States and other countries to find new and better ways to meet the world's increasing needs for energy while reducing greenhouse gas emissions. The need for sustainable energy with little greenhouse gas emissions has led to demonstration work in the production of hydrogen from biomass through steam reforming of pyrolysis gas and pyrolysis liquids. Our research to date has demonstrated the ability to produce hydrogen from biomass under stable conditions.<sup>[1]</sup> Future large-scale renewable hydrogen production using non-oxidative technologies will generate co-products in the form of a solid sequestered carbon. This char and carbon ("C") material represent a form of sequestered C that decomposes extremely slow<sup>[2]</sup> and retains the bio-capture CO<sub>2</sub> for centuries.

The limitation of the use of this form of carbon is a profit centric use. It was apparent that additional value needed to be added to this material that would justify large-scale handling and usage. In 1990s, C in the form of CO<sub>2</sub>, accumulated at rates ranging from 1.9 to 6.0 Pg C/yr and increasing CO<sub>2</sub> levels by 0.9 to 2.8 ppm/yr.<sup>[3]</sup> The volume of waste and unused biomass economically available in the United States is over 314 gigatons per year<sup>[4]</sup>. Sequestering a small percentage as valued added carbon could significantly reduce the atmospheric loading of CO<sub>2</sub> while simultaneously producing hydrogen. Normally hydrogen is referred to as a zero emissions fuel, however from life cycle perspective it can be viewed as a negative emissions fuel. In order to accomplish this economically, the sequestered C must have a very large and beneficial application such as a soil amendment and/or fertilizer.

The concept of utilizing charcoal as a soil amendment is not new. Man-made sites of charcoal rich soils intermingled with pottery shards and human artifacts have been identified covering 50,000 hectares of the Central Amazon rainforest each averaging 20ha and the largest at 350ha.<sup>[5]</sup> The radiocarbon dating of the sites have shown ages dating back 740–2,460 years BP<sup>[6]</sup> and 30% of the soil organic matter is made up of pyrolytic black carbon which is 35 times higher than the adjacent poorer quality soils (Oxisols)<sup>[7]</sup>. Most terra preta sites are identified by their thick black layers of soil (40-80cm) and some have been found in layers up to 2 meters thick<sup>[8]</sup>. These soils are so rich and fertile that they are dug up and sold as potting soil<sup>[9]</sup>. The current agricultural methods of the Kayapó (an ancient people with little European contact until the 19<sup>th</sup> century) has changed little and give evidence to the man-made techniques (slow burning fields and biomass) for creation of this fertile and sustainable method of agriculture which can be farmed intensively for up to 11 years.<sup>[10]</sup> This ability to farm soils without fertilization for many years is an anomaly in the rainforest. Despite the abundance of rainforest growth, their red and yellow soils are notoriously poor: weathered, highly acidic, and low in organic matter and essential nutrients.

### Experimental Project Description

The approach<sup>[11]</sup> in our research applies a pyrolysis process that has been developed to produce charcoal like by-product and synthetic gas (containing mainly H<sub>2</sub> and CO<sub>2</sub>) from biomass, which could come from

both farm and forestry sources. In this novel system<sup>[12]</sup>, a portion of the hydrogen is used to create ammonia where economical, or ammonia is purchased leaving hydrogen for fuel utilization. The ammonia is then combined with the char, H<sub>2</sub>O and CO<sub>2</sub>, at atmospheric pressure and ambient temperature to form a nitrogen enriched char. The char materials produced in this process contains a significant amount of non-decomposable carbons such as the elementary carbons that can be stored in soil as sequestered C. Furthermore, the carbon in the char is in a partially activated state and is highly absorbent. Recent research has shown that lower temperature charcoal produced at 500°C adsorbed 95% of ammonia versus charcoal produced at 700°C and 1000°C which had higher surface areas but only adsorbed 40%<sup>[13]</sup>. Matsui noted that acidic functional groups such as carboxyl were formed from lignin and cellulose at 400°C -500°C.<sup>[14,15]</sup> Charcoals, regardless of biological source, were found to form acidic functional groups at these temperatures which will preferentially adsorb base compounds such as ammonia and that the chemical adsorption plays the primary role over surface area. This research points to the carbonization conditions as a key ingredient in optimizing a charcoal as a nutrient carrier and binding compound for ammonia. Thus when used as a carrier for nitrogen compounds (such as NH<sub>4</sub><sup>+</sup>, urea or ammonium bicarbonate) and other plant nutrients, the char binding forms a slow-release fertilizer that is ideal for green plant growth. A combined NH<sub>4</sub>HCO<sub>3</sub>-char fertilizer is probably the best product that could maximally enhance sequestration of C into soils while providing slow-release nutrients for plant growth.

A flue gas scrubbing process<sup>[16,17]</sup> utilizing hydrated ammonia was tested in combination with a low temperature char. This approach utilized a chemical process, to directly capture greenhouse gas emissions at the smokestacks by converting CO<sub>2</sub>, NO<sub>x</sub>, and SO<sub>x</sub> emissions into valued added fertilizers (mainly NH<sub>4</sub>HCO<sub>3</sub>, ~98% and (NH<sub>4</sub>)<sub>2</sub>SO<sub>4</sub> and NH<sub>4</sub>NO<sub>3</sub>, <2%). These fertilizers can potentially enhance crop growth for sequestration of CO<sub>2</sub> and reduce NO<sub>3</sub><sup>-</sup> contamination of groundwater. As discussed above, the low temperature charcoal forms surface acid groups, which adsorbs and binds ammonia to the porous media for nucleation of CO<sub>2</sub>. When used as a scrubbing agent with fossil fuel exhaust, a mechanically fluidized cyclone creates a fertilizer-matrix with a commercially acceptable amount of nitrogen and a high percentage of very stable C. In addition, the inorganic carbon component (HCO<sub>3</sub><sup>-</sup>) of the NH<sub>4</sub>HCO<sub>3</sub> fertilizer is non-digestible to soil bacteria and thus can potentially be stored in certain soil (pH > 7.9) and subsoil terrains as even more sequestered C. This community-based solution operates as a closed loop process, integrating C sequestration, pollutant removal, fertilizer production, increased crop productivity and restoration of topsoil through the return of carbon and trace minerals. The benefits of producing a value added sequestering co-product from coal fired power plants and other fossil energy producing operations, can help bridge the transitions to clean energy systems that are in harmony with the earth's ecosystem.<sup>[18]</sup> An important benefit of this approach to the power industry is that it does not require compressors or prior separation of the CO<sub>2</sub>. The use of biomass in combination with fossil energy production, can allow agriculture, and the agrochemical industry infrastructure to assume a more holistic relationship of mutual support in helping each meet Kyoto greenhouse gas reduction targets.

The char component of the material acts to provide the same benefits as in terra preta sites reducing the leaching of soluble nutrients.<sup>[19]</sup> This increases plant growth, nutrient uptake and reduces nitrogen runoff. One experimental goal of the project was to identify process parameters that would produce a carbon material optimized for agricultural use. Since it has been shown that the charcoal addition from 2000 years ago is still providing significant soil fertility benefits<sup>[20]</sup> and farmers report up to three times crop yields over immediately adjacent non-terra preta soils. Recent research, conducted by Steiner, on the addition of charcoal to non terra preta soils<sup>[21]</sup> showed significant crop yield increases.

Charcoal has been found to support microbial communities<sup>[22]</sup> even greater than activated carbon (which is charcoal processed at higher temperatures with steam). Prior researchers assumed that the porous structure provided safe haven but we propose that it may be the availability of microbial nutrients. The processes of pyrolysis create an intrapore deposition of organic polycondensates<sup>[23]</sup>. The deposition of these materials may increase microbial activity.<sup>[24]</sup>

## Experimental Set-up and Results

**SEM Investigation of a Low Temperature Char.** The low temperature char particles are hydrophobic in nature and grind easily. The internal gases that escape from the material during the charring help develop charcoals natural porosity. The evolution of this adsorbent material provides a porous internal structure as well. We selected 400 °C as the target temperature for the char before being discharged from the pyrolysis reactor. The resulting char was cooled for 24 hours then fed through a two-roll crusher and then sieved with a mechanized screen through 30 mesh and 45 mesh screens. The resulting fraction remaining above the smaller screen was chosen as our starting material.

**SEM Investigation of an Enriched Carbon, Organic Slow-release Sequestering (ECOSS) Fertilizer.** Bench scale demonstrations by Oak Ridge National Laboratory recently demonstrated the removal of flue-gas CO<sub>2</sub> via formation of solid NH<sub>4</sub>HCO<sub>3</sub> through ammonia carbonation in the gas phase.<sup>[25]</sup> The results indicated that it is possible to use NH<sub>3</sub>+H<sub>2</sub>O+CO<sub>2</sub> solidifying process in gas phase to remove greenhouse-gas emissions from industrial facilities such as a coal-fired power plant. A study of agriculturally optimized charcoal produced by Eprida were combined with the above process created via the sequestration of a CO<sub>2</sub> stream. It was proposed that the char could act as a catalyst (providing more effective nucleation sites) to speed up the formation of solid NH<sub>4</sub>HCO<sub>3</sub> particles and enhance the efficiency of the gas phase process. A pilot demonstration was constructed to evaluate production and material characteristics of the NH<sub>4</sub>HCO<sub>3</sub>-char product. The process also showed promise that it could remove SO<sub>x</sub> and NO<sub>x</sub>, enhance sequestration of carbon into soils; providing an ideal "Enriched Carbon, Organic Slow-release Sequestering" ("ECOSS") fertilizer and nutrient carrier for plant growth. The value would be enhanced if the production of NH<sub>4</sub>HCO<sub>3</sub> could be developed inside the porous carbon media.

To test the production of a charcoal- NH<sub>4</sub>HCO<sub>3</sub> fertilizer, we used a mechanical fluidized cyclone, easily adaptable to any gas stream and injected CO<sub>2</sub>, and hydrated ammonia. A 250g charge of 30-45 mesh 400 °C char was fed in at regular intervals varying from 15-30 minutes. A higher rotor speed increased the fluidization and suspended the particles until they became too heavy from the deposition of NH<sub>4</sub>HCO<sub>3</sub> to be supported by fluidized gas flows.

**SEM Investigation of the Interior of an ECOSS-15 Char Particle.** The material produced was evaluated by scanning electron microscopy. The examinations revealed The very small molecules of NH<sub>3</sub>.H<sub>2</sub>O (hydrated ammonia) are adsorbed into the char fractures and internal cavities. As CO<sub>2</sub> enters, it converts the NH<sub>3</sub>.H<sub>2</sub>O into the solid NH<sub>4</sub>HCO<sub>3</sub>, trapping it inside the microporous material. The SEM's of the original char and the resulting product clearly evidenced the intra-pore development of the fibrous NH<sub>4</sub>HCO<sub>3</sub> inside the carbon-charcoal framework. The material accumulated as internal flat-top volcano like structures. This demonstration of the process showed that we can deposit nutrients inside the porous media using a low cost gas phase application. We analyzed the required amounts of hydrogen, reformed from biomass, which would be required as ammonia and calculated that 31.6% of the H<sub>2</sub> would be necessary for ECOSS production leaving (using all charcoal available from the process) leaving 68.4% of the hydrogen for use as a fuel.

The amount of C, directly converted from exhaust CO<sub>2</sub> is equal to 15.2% of the total sequestered carbon as a ammonium bicarbonate and for each 100kg of biomass, we will produce a total of 28.3kg of utilized carbon. In acid soils, this part of the carbon will convert to CO<sub>2</sub> but in alkaline soils, (pH>8) it will mineralize and remain stable. According to USDA reports, 60-70% of worldwide farmland is alkaline, so conservatively allowing for 50% of the bicarbonate to convert to CO<sub>2</sub>, this will leave us with approximately 25 kg of stable carbon in our soils for each 100kg of biomass processed. This carbon represents 91.5 kg of CO<sub>2</sub> of which 88% is stored as a very beneficial and stable charcoal. A different way to look at this is to compare the amount of energy produced and the resulting CO<sub>2</sub> impact. With 6.78 kg hydrogen extra produced per 100 kg of biomass, then 25/6.78 = 3.69 kg C/ kg H or 3.66x3.69=13.5 kg CO<sub>2</sub> / kg of hydrogen produced and used for energy. From a power perspective, that is 13.5kg CO<sub>2</sub> / 120,000 KJ of hydrogen consumed as a renewable energy or 112 kg/GJ of utilized and stored CO<sub>2</sub>.

## Global Potential

The large majority of increases in CO<sub>2</sub> will come from developing countries and a sustainable technology needs to be able to scale to meet the growing population needs. The second point is that The energy from a total systems point of view could create a viable pathway to carbon negative energy as detailed in the IASA focus on Bioenergy Utilization with CO<sub>2</sub> Capture and Sequestration (BECS)<sup>[26]</sup>. The effects (i.e. providing 112kg of CO<sub>2</sub> removal for each GJ of energy used) could allow major manufacturers to offset their carbon costs. For a quick test of reasonableness, if we take the atmospheric rise of 6.1GT and divide by 112kg/Gj = 54.5EJ. This number falls amazingly along the 55EJ estimate of the current amount of biomass that is used for energy in the world today.<sup>[27]</sup> While the potential reaches many times this for the future utilization of biomass, this shows that there is a chance that we can be proactive in our approach. Economic projections of a study based on the ORNL process were compared to this process. Equivalent 20% CO<sub>2</sub> reductions and credits needed to return a 33% ROI was estimated to cost \$46 million for a 700MW facility utilizing purchased ammonia. However, if the market for nitrogen were an upper limit, and renewable hydrogen were used for producing the worlds ammonia, and all the world's N fertilizer requirements were met from NH<sub>4</sub>HCO<sub>3</sub> scrubbed from power plant exhaust, then the total carbon capture at (1999 N levels) then coal combustion CO<sub>2</sub> could be reduced by ~39.9%. The factors of increased biomass growth with the addition of charcoal as found by Mann<sup>[28]</sup>, Hoshi<sup>[29]</sup>, Glaser<sup>[30]</sup>, Nishio<sup>[31]</sup>, and Ogawa<sup>[32]</sup> show increase biomass growth from 17% to as 280% with non-optimized char. The direct utilization of an optimized char plus slow release nitrogen/nutrients may allow the increase biomass growth targets worldwide. A portion of this increased biomass growth will be converted to soil organic matter, further increasing C capture (especially if no-till management practices are adopted).

The ability to slow down the release of ammonia in the soil will allow plants to increase their uptake of nitrogen. This will lead to a reduction in NO<sub>2</sub> atmospheric release. For each ton of nitrogen produced, 0.32 tons of C are released, and the 80.95 million tons of nitrogen utilized would represent 26 million tons of C. This is a small a small number in relative terms to the amounts released by combustion of coal (2427 million tons)<sup>[33]</sup>, however if we assume<sup>[34]</sup> 1.25% of our nitrogen fertilizer escapes into the atmosphere as N<sub>2</sub>O, then 1.923 million tons of N<sub>2</sub>O are released, with an CO<sub>2</sub> equivalence of 595.9 million tons or 162.5 million tons of C equivalent.

The economics of hydrogen from biomass has been addressed in the 2001 report by Spath<sup>[35]</sup>. Our analysis shows that inside plant use of renewable hydrogen would no longer be 2.4-2.8 times the costs from methane, but is approaching 1.6-1.9 times with the increase in natural gas prices. Since market price of nitrogen increases with natural gas prices and this process shows intra plant usage of renewable hydrogen (i.e. no storage or transport expense) becomes significantly more competitive at our current natural gas prices. A review of traditional ammonia processing, shows that due to unfavorable equilibrium conditions inherent in NH<sub>3</sub> conversion, only 20-30% of the hydrogen is converted in a single pass. We determined that the ECOSS process could only utilize 31.6% of the hydrogen as we were limited by the total amount of char produced and the target 10% nitrogen loading. This means that a single pass NH<sub>3</sub> converter could be used and the expense of separating and recycling unconverted hydrogen is eliminated. The 68.4% hydrogen is then available for sale or use by the power company/fertilizer partnership. This last bracket shows that the ECOSS process thus favors the inefficiencies of ammonia production and reduces costs inherent in trying to achieve high conversion rates of hydrogen.

## Conclusions

This concept of biomass energy production with agricultural charcoal utilization may open the door to millions of tons of CO<sub>2</sub> being removed from industrial emissions while utilizing captured C to restore valuable soil carbon content. This process simultaneously produces a zero emissions fuel that can be used to operate farm machinery and provide electricity for rural users, agricultural irrigation pumps, and rural industrial parks. The use of value added carbon while producing hydrogen (or energy) from biomass can lead to energy with an associated carbon credit (ie negative carbon energy). With this development non-renewable of carbon dioxide producers

can work with agricultural communities to play a significant part in reducing greenhouse gas emissions while building sustainable economic development programs for agricultural areas in the industrialized and economically developing societies.

**Acknowledgements.** Kim Magrini, Stefan Czernik, Bob Evans and Calvin Fiek and Don Reicosky and James Lee who have been seeking solutions to our CO<sub>2</sub> buildup. Thanks to Nigel Smith, Bruno Glaser, Christoph Steiner, Johannes Lehman, Bill Woods, Bill Denevan and Susanna Hecht who has taught us with the history of terra preta and finally Michael Obersteiner for his encouragement.

#### Literature Cited

<sup>1</sup> Day, D., Activities web report of a 100 hour production run of hydrogen from biomass in Blakely, GA, USA; 2002 <http://www.eprida.com/hydro/>  
<sup>2</sup> Gavin, D.G., Brubaker, L.B., and Lertzman, K.P. Holocene fire history of a coastal temperate rain forest based on soil charcoal radiocarbon dates. In press for Ecology: 2003

<sup>3</sup> IPCC, "Climate change 2001: the scientific basis", Intergovernmental Panel on Climate Change, 2001 (see also at [http://www.grida.no/climate/ipcc\\_tar/wg1/index.htm](http://www.grida.no/climate/ipcc_tar/wg1/index.htm).)

<sup>4</sup> Walsh, Marie et al., Biomass Feedstock Availability in the United States: 1999 State Level Analysis, 1999 <http://bioenergy.ornl.gov/resource/index.html>

<sup>5</sup> Glaser et.al, The 'Terra Preta' phenomenon: a model for sustainable agriculture in the humid tropics, *Naturwissenschaften* **2001**, 88: 37-41

<sup>6</sup> Saldarriaga JG, West DC, Holocene fires in the northern Amazon basin. *Quat Res* **1986**, 26: 358-366

<sup>7</sup> Glaser, et. al., Black Carbon in the Terra Preta Soils of the Brazilian Amazon Region, Proceedings 9th Annual V.M.Goldschmidt Conference, Cambridge, MA 1999, #7391

<sup>8</sup> Smith NJH, Anthrosols and human carrying capacity in Amazonia. *Ann Assoc Am Geogr* **1980**, 70: 553-566

<sup>9</sup> Mann, C., The Real Dirt on Rainforest Fertility, *Science* **2002**; 297:920-923

<sup>10</sup> Hecht, S and D. Posey. "Preliminary Results on Soil Management Techniques of the Kayapó Indians." *Advances in Economic Botany* **1989**, 7: 174-188.

<sup>11</sup> Y. Yeboah, et al., Hydrogen from Biomass for Urban Transportation, Proceedings of the 2002 US DOE Hydrogen Program Review

<sup>12</sup> Day, Danny; Robert Evans, James Lee U.S. Patent Application, 2002

<sup>13</sup> Asada, T. et al, Science of Bamboo Charcoal: Study on Carbonizing Temperature of Bamboo Charcoal and Removal Capability of Harmful Gases, *Journal of Health Science* **2002**, 48(6) 473-479

<sup>14</sup> Matsui, T. et al, Preparation and Analysis of Carbonization Products from Sgi, *Cryptomra japonica* D. Don) Wood. *Nippon Kagakukaishi* **2000**; 1:53-61 (Japanese)

<sup>15</sup> Nishimaya, K. et al., Analysis of Chemical Structure of Wood Cjrcoal by X-ray photoelectron spectroscopy **1998**, *Journal of Wood Science*, 44, 56-61

<sup>16</sup> Lee, J. W.; Li, R., A Novel Strategy for CO<sub>2</sub> Sequestration and Clean Air Protection, Proceedings of First National Conference on Carbon Sequestration, Washington, DC, May 1417, **2001**.

[http://www.netl.doe.gov/publications/proceedings/01/carbon\\_seq/p12.pdf](http://www.netl.doe.gov/publications/proceedings/01/carbon_seq/p12.pdf)

<sup>17</sup> Lee, J. W.; Li, R., Method for Reducing CO<sub>2</sub>, CO, NO<sub>x</sub>, and SO<sub>x</sub> Emissions, 1998 Oak Ridge National Laboratory Invention Disclosure, ERID 0631; 2002 U.S. Patent No. US 6,447,437 B1.

<sup>18</sup> Lee, J. W., and R. Li, Integration of Coal-Fired Energy Systems with CO<sub>2</sub> Sequestration through NH<sub>4</sub>HCO<sub>3</sub> Production, *Energy Conversion Management* **2003**; 44: 1535-1546.

<sup>19</sup> Schleppei P., Bucher-Wallin I., Siegwolf R., Saurer M., Muller N. & Bucher J.B., Simulation of increased nitrogen deposition to a montane forest ecosystem: partitioning of the added N; *Water Air Soil Pollution* **1999**; 116: 129-134

<sup>20</sup> Glaser B., Lehmann J., Zech W. Ameliorating physical and chemical properties of highly weathered soils in the tropics with charcoal – a review. *Biology and Fertility of Soils* **2002**; 35: 219-230.

<sup>21</sup> Wardle, D. A. et al., The charcoal effect in Boreal forests: mechanisms and ecological consequences, *Oecologia* **1998**; Volume 115 Issue 3: 419-426

<sup>22</sup> Pietikäinen, Janna, Soil microbes in boreal forest humus after fire (thesis 1999)

<http://ethesis.helsinki.fi/julkaisut/maa/mekol/vk/pietikainen/soilmicr.html>

<sup>23</sup> Runkel, R.O.H and Wilke, K, Chemical composition and properties of wood heated at 140C to 200C in a closed system without free space. Part II Holz als Roh und Werkstoff **1951**; 9: 260-270 (Ger.)

<sup>24</sup> Godsy, E. Michael, Impact of Human Activity on Groundwater Dynamics (Proceedings of a symposium held during the Sixth IAHS Scientific Assembly at Maastricht, The Netherlands, July 2001). IAHS Publication no. 269, 2001, pp. 303-309.

<sup>25</sup> Li, E. Hagaman, et al., "Removal of carbon dioxide from flue gas by ammonia carbonation in the gas phase," *Energy & Fuels* **2003**; 17: 69-74.

<sup>26</sup> Obersteiner, et al., Biomass Energy, Carbon Removal and Permanent Sequestration - A 'Real Option' for Managing Climate Risk, Report no. IR-02-042, Laxenburg, Austria: International Institute for Applied Systems Analysis, 2002.

<sup>27</sup> Hall, D.O., F. Rossillo-Calle, R.H. Williams and J. Woods,; Biomass for energy: Supply prospects. In: *Renewable Energy: Sources for Fuel and Electricity* [Johansson, T.B., H. Kelly, A.K.N. Reddy, and R.H. Williams (eds.)]. Island Press, Washington, D.C., 1993:593-652

<sup>28</sup> Mann, C., The Real Dirt on Rainforest Fertility, *Science* **2002**; 297:920-923

<sup>29</sup> Hoshi, T. (web report of growth studies with charcoal amendments on green tea yields) **2002** <http://www.fb.u-tokai.ac.jp/WWW/hoshi/cha>

<sup>30</sup> Glaser, et.al, Potential of Pyrolyzed Organic Matter in Soil Amelioration, 12th ISCO Conference, China, **2002**; 3:421

<sup>31</sup> Nishio, M., Microbial Fertilizers in Japan, Bulletin by National Institute of Agro-Environmental Sciences, Japan, **1999**

<sup>32</sup> Ogawa, M., Effect of charcoal on the root nodule and VA mycorrhizal formation of soybean, Proceedings of the Third Inter-national Mycology Congress, Tokyo, Ja-pan, **1983**: 578

<sup>33</sup> World Carbon Dioxide Emissions from the Consumption of Coal, 1992-2001 <http://www.eia.doe.gov/emeu/iea/tableh4.html>

<sup>34</sup> Mosier, et.al, Closing the Global N<sub>2</sub>O budget: Nitrous Oxide Emissions through the Agricultural Nitrogen Cycle, Nutrient Cycling and in Agro Ecosystems **1998**, 52: 223-245

<sup>35</sup> Spath, et al, Update of Hydrogen from Biomass -Determination of the Delivered Cost of Hydrogen, National Renewable Energy Laboratory, Milestone Report for the U.S. Department of Energy's Hydrogen Program 2001, United States

# PRODUCTION OF HYDROGEN FROM VEGETABLE OIL

Ross A.B., Dupont V., Hanley I., Jones J.M., Twigg M.V.

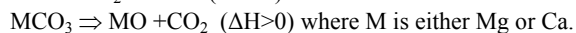
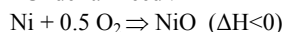
Energy and Resources Research Institute, The University of Leeds  
Leeds, LS2 9JT, UK.

## Introduction

The production of hydrogen from biomass and bio-oils represents a realistic renewable source. The development of the bio-diesel infrastructure could enable hydrogen to be produced from vegetable oil derived materials by either decentralised stationary reformers or on-board fuel processors.

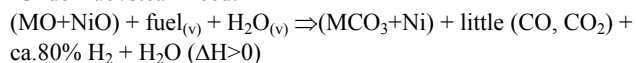
Unmixed steam reforming first proposed by Kumar, Lyon and Cole [1], is an emerging concept for enhancing the steam reforming process. It encompasses the concepts of unmixed combustion, regenerative sorption assisted steam reforming, and is potentially autothermal. It can be operated on a smaller scale to conventional steam reforming at lower pressures. The process operates in two steps forming a cycle. Firstly, an oxygen mass transfer catalyst is oxidised under air flow. In this study, the catalyst is Ni-based and its oxidation results in the formation of NiO compounds. The reaction is exothermic and heats up evenly the reactor bed. During this step, the reactor also contains a carbonate, here a Spanish dolomite (50/50% CaCO<sub>3</sub>/MgCO<sub>3</sub>). Some of the heat evolved during the Ni oxidation is used to decompose the carbonate, releasing the CO<sub>2</sub>. Secondly, the air feed is discontinued and is switched to the fuel/steam mix. Upon contact with the hot catalyst bed, the steam reforming reaction progresses, and CH<sub>4</sub>, CO, CO<sub>2</sub>, and H<sub>2</sub> are evolved. Under this step, the NiO reduces back to Ni while there is CO<sub>2</sub> capture on the adsorbent. The latter shifts the equilibrium of the water gas reaction toward increased hydrogen production. Hydrogen production is therefore intermittent, and for a continuous hydrogen yield, at least two identical reactor beds would need to run in parallel, each operating out of step. The cycle of reactions involved in the unmixed reforming process of an oxygenated hydrocarbon fuel such as vegetable oil is postulated below:

- Under air feed :



The gas product from this half cycle is an O<sub>2</sub>-depleted, CO<sub>2</sub>-rich air stream.

-Under fuel/steam feed:



For sunflower oil fuel, the elemental composition is taken to be C<sub>18</sub>H<sub>34.4</sub>O<sub>2.1</sub>.

The benefits of this process include an evenly heated reactor bed across its whole cross section, two product streams being either H<sub>2</sub> or CO<sub>2</sub> rich, low sensitivity to coking, low sensitivity to sulphur poisoning, autothermal behaviour, and, when running on a renewable fuel, no net-CO<sub>2</sub> emissions.

## Experimental

Following a period of catalyst and CO<sub>2</sub>-adsorbent screening using a micro-reactor [2], the bench scale demonstration unit of unmixed reforming described in **Figure 1** was designed to run on either methane or vegetable oil. The unit operates at pressures between 1-2 bar. The reactor temperature is maintained within the region of 600-800°C, initially by means of an external heating coil,

which can be phased out in the event of autothermal operation setting-in.

The liquid flow rates of oil or water are maintained within the range 0-3.2 ml/min depending on conditions. The two feed flows are preheated at 400°C, the temperature at which vegetable oil is completely vapourised. For a more detailed description of the reactor and its operation we refer the reader to [3]

During the fuel step a flow of either nitrogen diluted methane or nitrogen and vapourised vegetable oil mixture pass through the reactor together, this is then switched to air during the oxidative step. When using CH<sub>4</sub> and N<sub>2</sub> as the fuel feed, the inlet flows are 200 and 600 sccm respectively. When using sunflower oil, the liquid flow is 0.57 ml/min. Various steam to carbon ratios were studied.

The product gases are cooled using a water cooled condenser before entering a water trap followed by a chemical water trap (silica gel). The dry gaseous products are fed through a series of analysers. The gas volume concentrations of CO, CO<sub>2</sub>, CH<sub>4</sub>, H<sub>2</sub> and O<sub>2</sub> were monitored online using analysers from ABB. The gas reaching the analysers was dry and at room temperature.

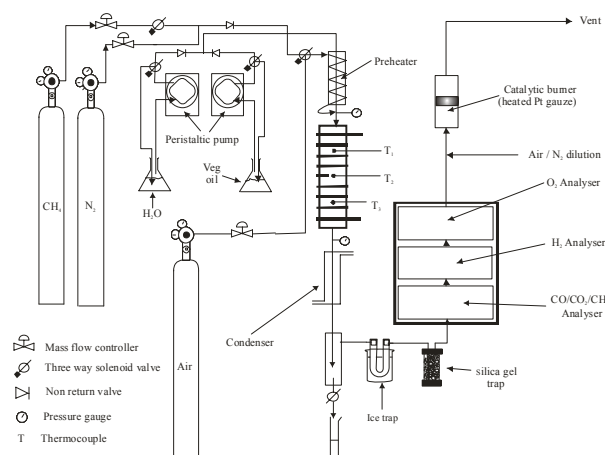


**Figure 1.** Schematic diagram of bench scale unmixed reforming reactor.

## Results and Discussion

### H<sub>2</sub> production under fuel feed

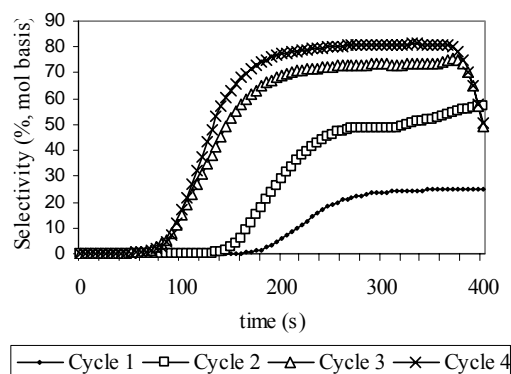


**Figure 2.** Selectivity to H<sub>2</sub> (%) with varying steam/carbon ratio during the methane feed step experiments when there is no CO<sub>2</sub> adsorbent in the reactor. Cycle 1 has no steam, cycles 2, 3, and 4 have steam/C of 1.65, 3.3 and 4.95 respectively. Water produced in the reactor makes for the balance to 100 %.

Because the peak dry H<sub>2</sub> concentrations corresponding to **Figure 2** were quite low (10%, 16%, 25%, 27% respectively), due to the presence of the diluent N<sub>2</sub>, we choose to show how the selectivity to H<sub>2</sub> improved with the presence of steam in the feed. In **Figure 3**, the effect of reactor temperature for the non-diluted methane feed in the reactor containing the CO<sub>2</sub> adsorbent can be seen on the dry H<sub>2</sub> concentration.

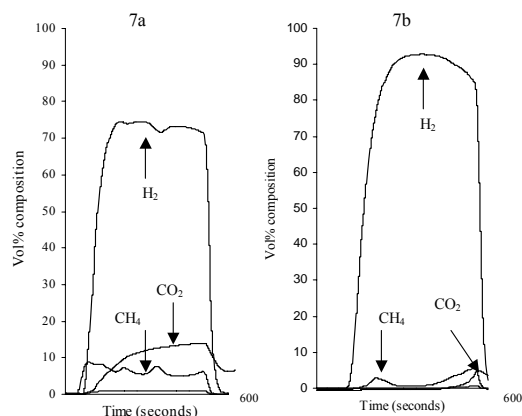


**Figure 3.** Typical dry gas composition of gaseous products during the fuel step for:-

- 7a. methane at 650°C, Steam/C of 4.  
7b. methane at 600°C, Steam/C of 4.

**Figure 3** a-b show that CO<sub>2</sub> and CH<sub>4</sub> dry gas concentrations are significantly reduced to the benefit of that of H<sub>2</sub> when the average reactor temperature of the fuel step is lowered from 650°C to 600°C. This indicates increased adsorption of CO<sub>2</sub> and the expected effect of shift in the water gas reaction. The extent to which CO<sub>2</sub> adsorption is maintained on a continuous basis is dependent upon the extent of regeneration of the adsorbent achieved during the previous oxidation cycle.

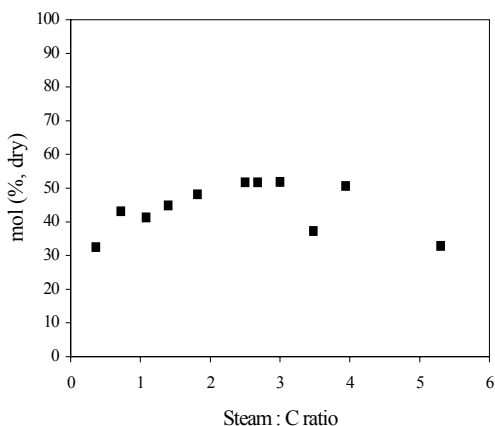


**Figure 4.** shows the effect of steam carbon ratio on the peak dry H<sub>2</sub> concentration when using a nitrogen (558 scm) and sunflower oil (0.57 ml/min) mix in a reactor containing just the Ni catalyst, in the absence of CO<sub>2</sub> adsorbent.

The points shown in **Figure 4** are the results of experiments carried out on three different days on the same catalyst. In spite of this, a clear trend can be picked up whereby the maximum dry H<sub>2</sub> concentration is obtained for steam carbon ratios between 2 and 4, as was found for methane fuel. However, the selectivity to H<sub>2</sub> when

using sunflower oil was of the order of few percent, hardly comparable to the methane experiments. This was concurrent with a production of water which was of the same order as the amount as the water reactant.

**Catalyst redox cycles under air and fuel feed.** Before we could attempt to operate the process autothermally, a major hurdle had to be overcome, namely the ability of the catalyst to reduce under the fuel feed and oxidize at similar rates under the air feed. Our first experiments with methane fuel indicated a rate of reduction two orders of magnitude slower than the oxidation rate, hence the subsequent experiments with sunflower oil were operated with an equivalent fuel molar rate two orders of magnitude larger than the methane. This had several effects. The reduction and oxidation rates were now both of the order of 10<sup>-4</sup> mol/s, but for a small adjustment. In counterpart, using a much larger fuel flow without changing the air feed had the effect of increased carbon formation by two orders of magnitude as well (order 10<sup>-4</sup> mol/s). This increased carbon formation was an additional oxygen sink to the nickel catalyst during the air feed which tended to produce CO and CO<sub>2</sub> in similar concentrations while it burned at a rate ca. 10<sup>-3</sup> mol/s. Under the previous lower methane flow, hardly any CO had evolved during the air feed, while all products of oxidation were NiO and CO<sub>2</sub>. Clearly, further optimization of the flows need to be carried out before the timing of the flows can be adjusted for autothermal operation.

### Conclusions

During the methane feed step, the main dry gas product was hydrogen. However, solid carbon is the main carbon product throughout the whole fuel feed step, while water is the principal hydrogen containing product during an initial phase. A much improved selectivity to H<sub>2</sub> product (up to 80%) is achieved when introducing steam in the feed. During the air feed step, the oxidation of Ni to NiO is slowed down by the carbon deposited during the previous fuel step. When operating with an adsorbent, the production of hydrogen is increased although the adsorption of CO<sub>2</sub> is sensitive to the bed temperature.

When using vegetable oil at a rate two orders of magnitude larger than in the methane experiments, chosen in order to achieve the desired NiO reduction rate, carbon formation is increased in proportion. The dry gas H<sub>2</sub> concentration is larger than with methane but the selectivity to H<sub>2</sub> much lower. The NiO reduction rate under fuel feed and the Ni oxidation rate under air feed are of similar magnitude, suggesting both feeds need little adjustment in the next optimisation phase of the process. Future work will focus on achieving autothermal operation in the reactor while maximizing the H<sub>2</sub> yield and the separation of the CO<sub>2</sub> from the H<sub>2</sub> product stream.

**Acknowledgement.** The work presented here was financially supported by the Engineering and Physical Science Research Council (EPSRC). The authors are also grateful to Mr Gavin Rickett and Dr Phil Ingram at Johnson Matthey.

### References

- (1) Kumar R. V.; Cole J. A.; Lyon R. K.; *Preprints of Symposia, J. Am. Chem. Soc.* 1999, 44, (4)
- (2) Ross A.B.; Dupont V.; Hanley I.; Ahmad O.S.; Jones J.M.; Twigg M.V. Proceedings of the 7<sup>th</sup> International Conference on Energy for a Clean Environment, 7-10 July 2003, Lisbon, Portugal.
- (3) Ross A.B.; Hanley I.; Dupont V.; Jones J.M.; Twigg M.V. Sixth International Conference in Science in Thermal and Chemical Biomass Conversion (STCBC), 30 Aug-2 Sept.2004, Victoria, B.C., Canada.

# SUSTAINABLE HYDROGEN FROM BIO-OIL - CATALYTIC STEAM REFORMING OF ACETIC ACID AS A MODEL OXYGENATE

Kazuhiro Takanabe, Ken-ichi Aika

Tokyo Institute of Technology, Interdisciplinary Graduate School of Science and Engineering, 4259 Nagatsuta, Midori-ku, Yokohama, 226-8502, Japan.

K. Seshan, and Leon Lefferts

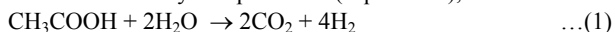
University of Twente, Institute of Mechanics, Processes and Control Twente (IMPACT), Faculty of Science and Technology, P.O. Box 217, 7500AE, Enschede, The Netherlands.

## Introduction

Hydrogen as a fuel has recently been an important issue due to developments in fuel cell technology. Hydrogen production from sustainable sources, e.g. biomass, is gaining attention for a CO<sub>2</sub> neutral energy supply. Recent developments in flash pyrolysis technologies make it possible to convert lignocellulosic biomass efficiently to a bio-oil, which is easier for handling and transport.<sup>1</sup> The bio-oil so generated contains a variety of aliphatic and aromatic oxygenates (aldehydes, ketones, acids, alcohols).

Combination of catalytic steam reforming and water gas shift reaction is the most promising option to generate hydrogen since these reaction steps maximize hydrogen yield. During steam reforming of bio-oil, deactivation due to coke/oligomer deposition on the catalysts is a severe problem. It has been reported<sup>2</sup> that deactivation is unavoidable even in the presence of excess steam (H<sub>2</sub>O/C > 5). Economically, lower steam/carbon (S/C) ratio (< 2) is preferable. In this study, Pt/ZrO<sub>2</sub> has been investigated since earlier work<sup>3</sup> has shown excellent activity and stability for Pt/ZrO<sub>2</sub> under conditions favorable for coke formation, for e.g., even in the absence of steam, during CO<sub>2</sub> reforming of natural gas.

Bio-oil is a mixture of oxygenates. In order to provide a knowledge base for the design of active and stable catalysts for steam reforming of bio-oil, studies have been initiated with model oxygenates. Acetic acid (HAc) has been chosen as a model compound in this study because it is a major component of bio-oil (up to 32 wt%).<sup>1</sup> It is known that steam reforming and water gas shift reaction (CO + H<sub>2</sub>O ⇌ CO<sub>2</sub> + H<sub>2</sub>) occur simultaneously and the overall stoichiometry is represented (Equation 1),



This study describes attempts to understand the reaction and deactivation mechanisms in order to establish guidelines for the design of efficient catalysts for steam reforming of bio-oil.

## Experimental

**Catalyst preparation.** Pt/ZrO<sub>2</sub> was prepared by wet impregnation technique<sup>3</sup>. Pt loading was set to 0.5 wt%. The catalyst was calcined at 925 K for 15 h.

**Catalytic measurements.** The amounts of 50 mg of catalysts were loaded in a fixed bed reactor and held by quartz wool plugs. The catalyst was first reduced in 5% H<sub>2</sub> in N<sub>2</sub> at 925 K for 1 hr. An aqueous solution of HAc giving a steam to carbon molar ratio (S/C) of 5 was introduced by using a microfeeder (KD Scientific) and a syringe (Hamilton co.). Gas mixture, HAc/H<sub>2</sub>O/N<sub>2</sub>/Ar, was fed to give a ratio of 3/30/5/82 ml min<sup>-1</sup> (N<sub>2</sub> as an internal standard). For analysis, a flame ionization detector (FID) and a Hayesep Q column were used for HAc, acetone, ketene, and hydrocarbons; a thermal conductivity detector (TCD) and a Carbosieve column were used for H<sub>2</sub>, N<sub>2</sub>, CO, CH<sub>4</sub>, and CO<sub>2</sub>.

Pulse experiments were performed with 20 mg of Pt/ZrO<sub>2</sub>. After reduction at 925 K, the system was purged in Ar at a flow rate of

37.5 ml min<sup>-1</sup>. Pulses of HAc aqueous solution (S/C = 5, 3.5 μmol of HAc) at 293 K were introduced.

The hydrogen yields were calculated based on Equation 1. For carbon containing compounds, the yields were calculated based on C1 equivalent values.

**Catalyst characterization.** Thermogravimetry (TG) (Mettler Toledo TGA/SDTA 851E) was used to determine the amount of deposits in the catalysts.

IR spectra were recorded *in situ* under vacuum in transmission mode (Bruker, Vector 22, MCT detector). The catalyst reduced *ex situ* at 925 K was mounted in the IR cell and firstly reduced *in situ* by introducing 0.1 mbar of H<sub>2</sub> at 725 K. After evacuation, oxygenates and steam were introduced into the system with an S/C molar ratio of 5 at a total pressure of 0.1 mbar at 725 K. Each spectrum consists of 32 scans taken at 4 cm<sup>-1</sup> resolution.

## Results and Discussions

**Figure 1** shows HAc conversion and yields of products during HAc/H<sub>2</sub>O reaction over Pt/ZrO<sub>2</sub>. Conversion was close to 100% and constant for 3 h, however, yields of products changed with time. In the beginning (5 min), H<sub>2</sub> and CO<sub>2</sub> were the main products, CH<sub>4</sub> and CO were observed in small quantities. H<sub>2</sub> yield (47%) was close to equilibrium value (56%). The product yields and pattern indicates that the catalyst was active for steam reforming. However, after 25 minutes time on stream, H<sub>2</sub> and CO<sub>2</sub> yields decreased drastically, and an increase in acetone was observed.

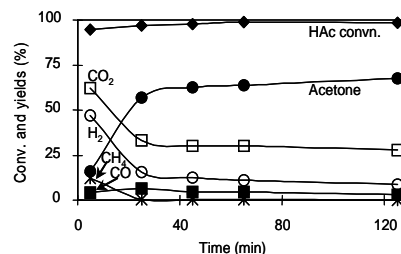


**Figure 1.** Conversion and yields for steam reforming of HAc over Pt/ZrO<sub>2</sub> catalyst. (725 K, S/C = 5, GHSV = 160000 h<sup>-1</sup>).

**Figure 2** shows HAc conversion and yields of products during HAc/H<sub>2</sub>O reaction over ZrO<sub>2</sub> (without Pt). HAc conversion was close to 90%. The conversion of HAc and yields of the products were constant for 3 h. However, no steam reforming activity (H<sub>2</sub> and CO) was observed, and only acetone and CO<sub>2</sub> were observed as products. HAc is known to convert to acetone easily and the reaction is catalyzed by a variety of oxides.<sup>4</sup> ZrO<sub>2</sub> is also known as such an oxide. The stoichiometry of the products observed (acetone and CO<sub>2</sub>, 1:1) correspond to the ketonization reaction (Equation 2).



Both Pt/ZrO<sub>2</sub> and ZrO<sub>2</sub> were very active for HAc conversion. However, H<sub>2</sub> and CO, i.e., steam reforming products were produced only over Pt/ZrO<sub>2</sub> and not over ZrO<sub>2</sub>. This implies that presence of Pt is essential for steam reforming. ZrO<sub>2</sub> shows acetone yields similar to those observed over Pt/ZrO<sub>2</sub> after 25 minutes time on stream (Figure 1), indicating that even after the active sites for steam reforming were deactivated, the accessible ZrO<sub>2</sub> sites still provided the activity to form acetone and CO<sub>2</sub>.

For Pt/ZrO<sub>2</sub> and ZrO<sub>2</sub>, TG experiments showed approximately 1.2 and 0.8 wt% deposits, respectively, after 3 hour test. Regeneration in air restored catalytic activity, indicating that blocking active sites by deposits caused deactivation of the Pt/ZrO<sub>2</sub> catalyst for the steam reforming.

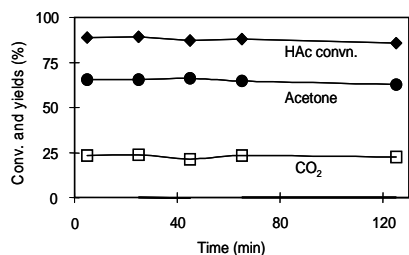


**Figure 2.** Conversion and yields for steam reforming of HAc over ZrO<sub>2</sub> catalyst. (725 K, S/C = 5, GHSV = 160000 h<sup>-1</sup>).

Presence of acetone in the product mixture and formation of deposits on ZrO<sub>2</sub> indicates a role for acetone in catalyst deactivation. Acetone is known to undergo aldol type condensation and give products such as diacetone alcohol, mesityl oxide (MO) and MO is known to form oligomers easily (CH<sub>3</sub>COCH<sub>3</sub> → (CH<sub>3</sub>)<sub>2</sub>C(OH)CH<sub>2</sub>COCH<sub>3</sub> → (CH<sub>3</sub>)<sub>2</sub>C=CHCOCH<sub>3</sub> → oligomers).<sup>5</sup> In order to check if these oligomers play a role in deactivation, kinetic and *in situ* IR measurements were carried out with Pt/ZrO<sub>2</sub> pre-exposed to MO.

**Table 1** shows comparison between HAc conversion and H<sub>2</sub> yield with or without MO treatment during pulse experiment. It is seen that Pt/ZrO<sub>2</sub> catalyst deactivated for H<sub>2</sub> formation (steam reforming) more rapidly when contacted with MO in comparison to HAc.

**Table 1. Comparison of HAc Conversion and H<sub>2</sub> Yield between Fresh and MO Treated Pt/ZrO<sub>2</sub>**

Catalyst (Pt/ZrO <sub>2</sub> )	HAc convn. (%)	H <sub>2</sub> yield (%)
Fresh	98.2	60.0
MO treated <sup>a</sup>	82.4	29.1

<sup>a</sup>MO/H<sub>2</sub>O pulse (0.32 μmol-MO, S/C = 5) was introduced before a HAc/H<sub>2</sub>O pulse.

*In situ* IR spectra recorded over Pt/ZrO<sub>2</sub> are shown in **Figure 3**. In the presence of HAc/H<sub>2</sub>O (**Figure 3a**) characteristic peaks for linear CO adsorbed on Pt at 2060 cm<sup>-1</sup> were observed. This confirms the production of CO in the *in situ* experiment. Additionally bands due to oxygenates (acetate, carbonate) derived from HAc (1541, 1426 and 1405 cm<sup>-1</sup>) were also seen. Exposure-evacuation cycles with HAc/H<sub>2</sub>O were repeated three times (not shown) and no significant difference in IR spectra were observed.

After pre-exposure to MO, *in situ* IR spectra were recorded with HAc/H<sub>2</sub>O (**Figure 3b**). The spectra showed similar oxygenate peaks on the support but the CO peak was very weak. This implies the activity towards CO formation (steam reforming) was deactivated as expected from kinetic experiments. However, when CO was introduced in the gas phase, the intensity of the peak for CO significantly increased (**Figure 3c**). This indicates that the Pt surface was not blocked completely even though the activity for steam reforming was lost. This further implies that only part of the surface Pt atoms are responsible for steam reforming. Since oligomerization reactions of MO occur on the support, and the fact that Pt sites were deactivated with MO, we conclude that the Pt sites active for steam reforming are at the close vicinity of the support. This is in agreement with a bi-functional mechanism proposed by us for the steam or CO<sub>2</sub> reforming of methane, where methane is activated on the metal and steam or CO<sub>2</sub> on the support, the reaction occurring at the metal support boundary.<sup>3,6</sup> Thus, ZrO<sub>2</sub> may have a key role in the mechanism for steam reforming in the activation of water. Once MO, or the oligomers derived from it, is formed on the support even in

small amounts, they could block the boundary sites and deactivate the Pt/ZrO<sub>2</sub> catalyst.

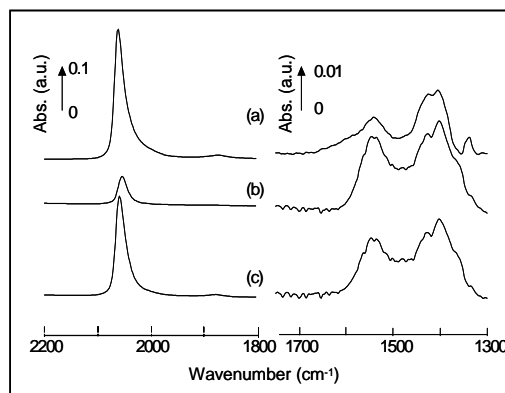


**Figure 3.** *In situ* IR spectra over Pt/ZrO<sub>2</sub> at 725 K (Steam/Carbon = 5, 0.1 mbar). (a) HAc/H<sub>2</sub>O, (b) HAc/H<sub>2</sub>O after MO/H<sub>2</sub>O treatment and evacuation, (c) CO treatment after (b) without evacuation

The acid-base properties of the support oxides play a key role in catalyzing the condensation reactions.<sup>5</sup> ZrO<sub>2</sub> has an important role in steam reforming *via* steam activation. However, condensation reaction could also happen over ZrO<sub>2</sub>. Thus, design of a stable catalyst should be aimed at improvement of the support, minimizing the condensation reactions as well as enhancing the steam activation capacity.

## Conclusions

The Pt/ZrO<sub>2</sub> catalysts showed high activities at initial time on stream, but lost its activity for steam reforming (H<sub>2</sub> production) rapidly.

Results obtained in the study point to a bifunctional mechanism for steam reforming of HAc on Pt/ZrO<sub>2</sub>, i.e., HAc activation takes place on Pt and steam activation on ZrO<sub>2</sub>. The reaction occurs at the Pt periphery in close proximity of ZrO<sub>2</sub>. The catalysts deactivate due to blocking of active sites by oligomers derived from HAc/acetone on ZrO<sub>2</sub>. In order to develop a durable catalyst, the oligomerization/condensation reactions which take place on the support need to be minimized.

**Acknowledgement.** One of us (K. Takanabe) thanks the Huygens exchange program (Nuffic, the Netherlands) for financial support. This work was performed under the auspices of NIOK, The Netherlands Institute for Catalysis.

## References

- (1) Milne, T.; Agblevor, F.; Davis, M.; Deutch, S.; Johnson, D. In *Developments in Thermochemical Biomass Conversion*; Bridgwater, A.V.; Boocock, D.G.B., Ed.; Blackie, 1997, pp. 409-424.
- (2) Wang, D.; Montané, D.; Chornet, E., *Appl. Catal. A*, **1996**, 143, 245-270.
- (3) Bitter, J.H.; Seshan, K.; Lercher, J.A., *J. Catal.* 1998, 176, 93-101.
- (4) Rajadurai, S., *Catal. Rev. -Sci. Eng.*, **1994**, 36, 385-403.
- (5) Iglesia, E.; Barton, D.G.; Biscardi, J.A.; Gines, M.J.L.; Soled, S.L., *Catal. Today*, **1997**, 38, 339-360.
- (6) Nagaoka, K.; Seshan, K.; Aika, K.; Lercher, J.A., *J. Catal.*, **2001**, 197, 34-42.

# DETERMINATION OF THE OXIDATION CHARACTERISTICS OF FIR (*Abies bornmulleriana*) WOOD

Ahu Gümrah Dumanlı, Billur Sakintuna, and Yuda Yürüm

Faculty of Engineering and Natural Sciences, Sabanci University,  
Tuzla, Istanbul 34956, Turkey

## Introduction

About 90% of the energy used by humankind is based on combustion – mainly combustion of fossil fuels (oil, coal, and natural gas), with a relatively small contribution from the combustion of biomass (wood). The main exceptions to combustion are nuclear fission and hydro for the generation of electricity. Energy conversion by combustion has a significant impact on the planet's atmosphere by means of ground-level air pollution (photochemical smog, acid rain, global climate change, and stratosphere particulate matter, SO<sub>2</sub>, CO, toxic organic gases and vapors and toxic metals), acid rain, global climate change, and stratosphere ozone depletion.

Although energy production from biomass residues is limited due to availability and high cost compared to fossil fuels<sup>1,2</sup>, biomass provides a renewable source of energy on a scale sufficient to play a significant role in the development of sustainable energy programmes, so vital if we are to create a greener, more ecologically sensitive society<sup>3,4</sup>.

By optimal utilization of biomass resources and development of new technical advances, biomass will become more efficient and competitive as an energy source. In order to consider the optimum conditions for biomass utilization one should start investigating the combustion characteristics of the biomass. In this study we aimed to find the combustion characteristics of wood samples as the starting point for the evaluation of use as an energy source.

## Experimental

The wood sample used in this work was a bark-free fir (*Abies bornmulleriana*) sawdust sample obtained from Bolu forests (northwest Anatolia) in Turkey. The proximate and elemental analyses of the wood sample were done at the Instrumental Analysis Laboratory of the Scientific and Technical Research Council of Turkey, Ankara, is given in Table 1. The sawdust was ground and sieved to below 175 µm (-80 mesh) size.

**Table 1. Proximate and Elemental Analyses of the Fir Wood Sample**

Proximate analysis, % (as received)	
Volatile matter	85.5
Fixed carbon	10.5
Moisture	3.7
Ash	0.3
Elemental analysis, % (daf)	
C	47.2
H	6.1
N	0.3
O (by difference)	46.7

**Characterization Techniques.** Combustion and decomposition characteristics of the wood sample were analyzed by using a Netsch 449C thermogravimetric analyzer (TGA). TGA

analysis was done in the following manner; the wood samples were heated up to a temperature range between 500°C and 1000°C with different heating rates of 5K/min, 10K/min, 20 K/min and 30 K/min. In addition to this, TGA analysis was combined with an Bruker Equinox 55 FTIR in order to monitor the released gases during combustion and decomposition. The ashes obtained from TGA analysis were examined with a Leo G34-Supra 35VP scanning electron microscope (SEM) and SEM images were compared with the images obtained from unburnt wood sample. Additionally the wood sample was objected to heat treatment at different temperatures between 100°C and 400°C. The mass loss according to the heat treatment was recorded and these samples were analyzed with an IKA-Calorimeter System-C4000-Adiabatic calorimeter, again included the comparison with the untreated sample.

## Results and Discussion

The heating rate seemed to be very effective on the oxidation of the samples and different mass losses were observed. There were two main temperatures for mass losses; as the heating rate was increased the greatest mass loss was detected at higher temperatures.

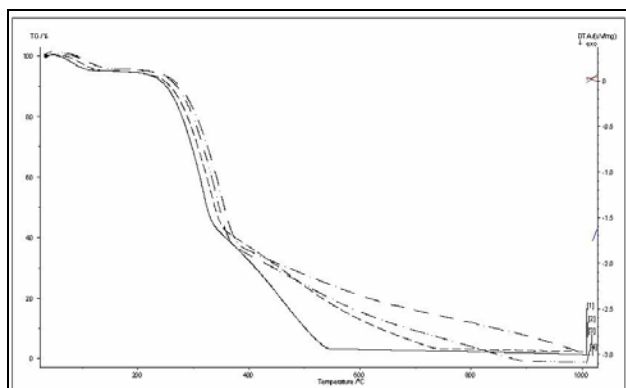


**Figure 1.** TGA traces of the wood samples.

**Table 2.** Percent Mass Loss and Change of Calorific Values

Heat Treatment Temperature, °C	Mass Loss, %	Calorific Value, kJ/kg
Unheated	-	18746
100°C	5.9	19135
200°C	11.0	19521
300°C	32.0	3149
400°C	99.3	-

While heat treatment of the wood sample up to 200°C increased the calorific value of the wood due the removal of the low volatile compounds. As the heat treatment temperature was increased to 300°C and higher temperatures due to the pyrolytic losses of carbonaceous material from the structure of the wood the calorific values decreased sharply.

The FTIR spectra of the volatiles obtained during TGA measurements are presented in **Figures 2-4**. The peaks due to CO<sub>2</sub> and H<sub>2</sub>O can be seen near 2335 cm<sup>-1</sup> and 3240 cm<sup>-1</sup>, respectively and a complex peak near between 1500- and 1700 cm<sup>-1</sup> is due to H<sub>2</sub>O.

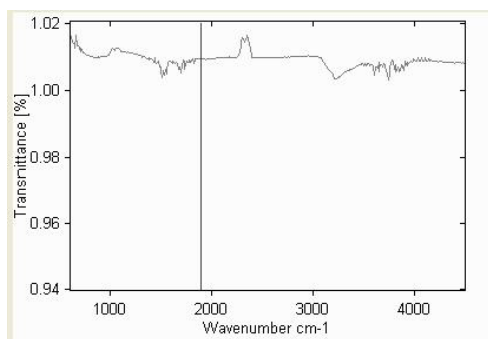


**Figure 2.** FTIR spectrum of the volatiles evolved at the 14<sup>th</sup> second during TGA measurement.

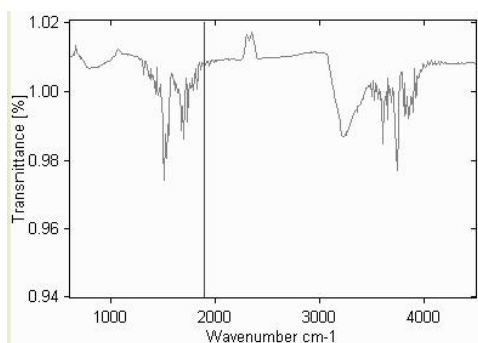


**Figure 3.** FTIR spectrum of the volatiles evolved at the 1506<sup>th</sup> second during TGA measurement.

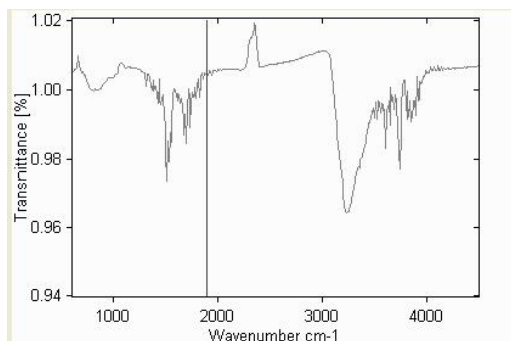


**Figure 4.** FTIR spectrum of the volatiles evolved at the 2041<sup>st</sup> second during TGA measurement.

SEM micrographs of the wood dust before and after oxidation are presented in the **Figure 5** and **6**. Fibrous structure of the wood was destroyed and a structure with a relatively greater porosity seemed to form after the oxidation experiments.

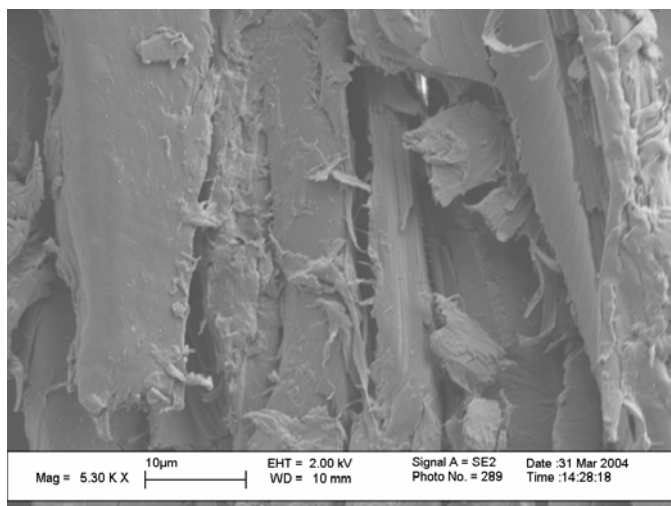


**Figure 5.** SEM micrograph of the wood dust before oxidation.

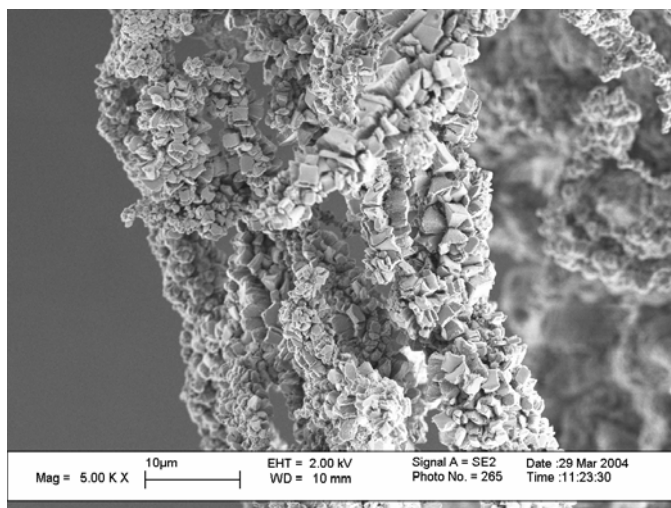


**Figure 6.** SEM micrograph of the wood dust after oxidation.

### Conclusions

The effect of heat treatment on the calorific values and structural changes of a wood sample before its oxidation was investigated by using a TGA system and scanning electron microscope. Heat treatment up to 200°C increased the calorific value of the wood. Structural changes during oxidation reactions observed indicated the loss of volatiles and production of porosity on the surface of the residue. The work is in progress and it is expected that the complete set of analysis of the material evolving during oxidation and changes in the morphology of the residual material of wood are being investigated in detail.

### References

1. Dornburg, V.; Faaij, A. P. C. *Biomass and Bioenergy* **2001**, *21*, 91-108.
2. Mc Gowin, C. R.; G.A., W. *Biomass and Bioenergy* **1997**, *10*, 167-175.
3. Holliday, L. *Ionic Polymers*; John Wileys & Sons: New York - Toronto, 1975.
4. Wahlund, B.; Yan, J.; Westermark, M. *Biomass and Bioenergy* **2003**, *26*, 531-544.

# THE EFFECT OF ANTIOXIDANT ADDITION ON NO<sub>x</sub> EMISSIONS FROM BIODIESEL

Melissa A. Hess, Michael J. Haas, Thomas A. Foglia, and William N. Marmer

United States Department of Agriculture, Agricultural Research Service, Eastern Regional Research Center  
600 E. Mermaid Lane  
Wyndmoor, Pennsylvania, 19038

## Introduction

Although the use of biodiesel offers many environmental advantages over petrodiesel, an increase in NO<sub>x</sub> emissions from biodiesel combustion, relative to levels observed from petrodiesel combustion, has been reported by several researchers. (1-3) This increase is of concern in areas that are subject to strict environmental regulations. For universal acceptance of biodiesel, it is desirable to reduce these NO<sub>x</sub> emissions at least to levels observed with petrodiesel combustion.

NO<sub>x</sub> can be formed by two major pathways during diesel fuel combustion: the Zeldovich (thermal) mechanism and the Fenimore ("prompt") mechanism. The rate of the Zeldovich reactions is flame temperature-dependent, whereas the Fenimore pathway is more complex. In the Fenimore mechanism, free radicals formed from the fuel react with N<sub>2</sub> to eventually form NO<sub>x</sub>. This takes place very early in the combustion process and is partly dependent upon the fuel radical concentration and how it is established. (4)

Some data have indicated that the chemical makeup of biodiesel can influence the amount of NO<sub>x</sub> formed during its combustion. McCormick *et al.* (5) published data that correlated the properties of various biodiesels to NO<sub>x</sub> emissions. One notable result was a strong positive correlation between the iodine value of the fuel (a function of the number of double bonds) and NO<sub>x</sub>: as iodine value increased, so did the NO<sub>x</sub> emissions. These data suggest a role of double bonds in elevating NO<sub>x</sub> output. Sites of unsaturation are known to have a greater propensity for radical formation than do carbon-carbon single bonds. It is conceivable that this increase in free radical generation is at the heart of the increase in NO<sub>x</sub> output by some biodiesels. If so, a quenching of free radicals during combustion may reduce or eliminate this NO<sub>x</sub> elevation. Antioxidants are known to be free radical quenching agents.

Acting on this postulate, McCormick *et al.* (6) added a common antioxidant, *tert*-butyl hydroquinone (TBHQ), to biodiesel as a possible method of NO<sub>x</sub> reduction. They observed a slight reduction in NO<sub>x</sub> and suggested that the use of antioxidants as a NO<sub>x</sub> mitigation strategy deserved more study. Moreover, the addition of antioxidants to biodiesel is being investigated to increase its storage stability and it is important to understand the impact that such addition may have on NO<sub>x</sub> formation.

## Experimental

**Materials.** Certified diesel fuel was obtained from Chevron Phillips Chemical Company (Houston, Texas). The fuel used was low sulfur (365 ppm), with a cetane number of 46.8. The biodiesel used was Soygold, a methyl soyate biodiesel purchased from Ag Environmental Products (Omaha, Nebraska) in one-gallon units to protect the fuel from extensive oxidation. 2-Ethylhexyl nitrate (2-EHN), 2,2'-methylenebis(6-*tert*-butyl-4-methylphenol), vitamin E, *tert*-butylhydroquinone, propyl gallate, diphenylamine, and butylated hydroxyanisole were purchased from Sigma-Aldrich Chemical Co. (St. Louis, Missouri). Structures of the antioxidants are shown in Figure 1.

The fuel used had a blend composition of 80% petrodiesel and 20% biodiesel (B20). Additives were tested at a level of 1000 ppm.

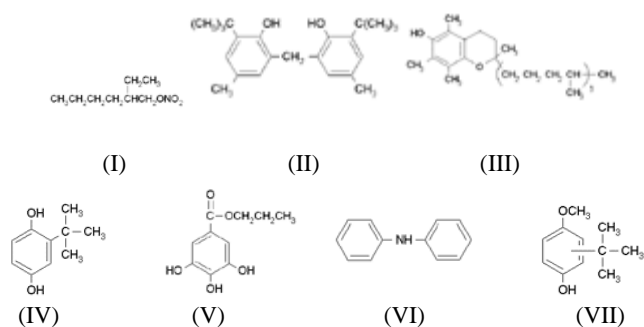


**Figure 1.** Structures of selected additives. (I) 2-ethylhexyl nitrate. (II) 2,2'-methylenebis(6-*tert*-butyl-4-methylphenol) (III) Vitamin E (IV) TBHQ (V) Propyl gallate (VI) Diphenylamine (VII) BHA

**Method.** A Yanmar L100 single cylinder, four stroke, naturally aspirated, direct injection diesel engine from Bowers Power Systems (Kent, Washington) was installed and instrumented for NO<sub>x</sub> measurements. The engine had a compression ratio of 20:1, a displacement of 0.418 L, and a fuel injection timing of 17±0.5 degrees before top dead center (bTDC). The engine was connected to an electrical generator. Load was added to the engine by using the generator to power work lights. The results discussed here are obtained at a load of 5 kW (82% maximum load) and an engine speed of 3200 rpm. These conditions were chosen to generate NO<sub>x</sub> levels high enough to allow small changes in NO<sub>x</sub> emission levels to be detected.

NO and NO<sub>2</sub> were measured using single gas monitors (model CA-CALC) manufactured by TSI Instruments (Shoreview, Minnesota). These monitors have electrochemical sensors as opposed to the chemiluminescence methods normally employed for NO<sub>x</sub> detection. The monitors were chosen for simplicity and affordability, and were calibrated frequently using calibration gases. Exhaust temperature was monitored using a thermocouple from Omega Instruments (Stamford, Connecticut) inserted into the exhaust gas stream.

Since the engine was minimally instrumented with no provisions for the control of such variables as inlet air temperature and humidity, the baseline numbers were generally not repeatable on a daily basis. Therefore, for each test, NO<sub>x</sub> emission levels from petrodiesel, B20, and B20 with the additive were measured against those fuels without the additive. An experiment began by bringing the engine to steady state using certified diesel fuel. The speed of the engine was monitored using a tachometer. The engine was held at a constant speed and load for the duration of the test and the NO<sub>x</sub> emissions of the petrodiesel were measured. A minimum of triplicate measurements were made to ensure an accurate NO<sub>x</sub> measurement. The fuel was then switched to B20 without disrupting the operation of the engine. The engine was run at steady state for a time sufficient to ensure that the petrodiesel was flushed from the system and that steady state had been achieved. The NO<sub>x</sub> emissions from B20 were then measured. The fuel was then switched to B20 containing 1000 ppm of the antioxidant additive again without disrupting engine operation. The engine was allowed to come to steady state and the NO<sub>x</sub> levels were measured again. Experiments were performed to ensure that when the fuel was switched back to B20, the same results as prior to running the additized blend were achieved. The NO<sub>x</sub> emission levels for the additized fuel were compared to the NO<sub>x</sub>

levels measured for B20 in that experiment only. The percent changes in NO<sub>x</sub> emissions from experiment to experiment were compared.

## Results and Discussion

The engine system employed here proved effective and reliable as a screening method to determine if antioxidant fuel additives have an effect on NO<sub>x</sub> levels. Candidate additives that show promise with such a system will be tested at a rigorous engine test facility in the future.

It was necessary to confirm that the reported difference in NO<sub>x</sub> emissions between biodiesel and petrodiesel could be observed. As shown in Table 1, a 6.2% increase in NO<sub>x</sub> emissions was observed when B20 was used as opposed to petrodiesel. The increase observed here was fairly consistent throughout the tests and is in agreement with results reported in the literature. (1-3)

It was also of interest to establish that reduction in NO<sub>x</sub> by the use of accepted NO<sub>x</sub>-lowering treatments could be attained. To accomplish this 2-EHN was added to the fuel at a 1000 ppm level. 2-EHN is known to be an effective additive for reducing NO<sub>x</sub> emissions at this level in a variety of diesel engines. (7,8) This additive increases the cetane number of the fuel, which leads to shorter ignition times that result in decreased NO<sub>x</sub> emissions. Again, the results observed here corroborate those seen by others; the addition of 2-EHN at 1000 ppm reduced NO<sub>x</sub> by 4.5%. This observation suggests that this engine system responds typically to a known NO<sub>x</sub> reducing agent.

The antioxidants were chosen based on several considerations. Several are readily available and inexpensive since they are used in the food industry to prevent lipid oxidation. Additionally, Mittelbach and Schober (9) performed a study in which antioxidants were rated for their effectiveness in terms of fuel stability. Antioxidants that they found to be effective (such as *n*-propyl gallate and TBHQ) were tested in hopes that these additives would serve two functions, namely increasing storage stability and reducing NO<sub>x</sub>.

Table 1 lists the effect of the addition of each of six antioxidants on NO<sub>x</sub> emissions during B20 combustion. The antioxidants used had minimal effect on NO<sub>x</sub> emissions, but the results from three antioxidants were notable.

**Table 1. Effect of Additive Addition on NO<sub>x</sub> Emissions**

Fuel	Change in NO <sub>x</sub> from B20 Levels
Diesel Fuel (B0)	-6.2%
B20 + 2-EHN	-4.5%
B20 + 2,2'-methylenebis(6-tert-butyl-4-methylphenol)	+0.2%
B20 + Vitamin E	+0.3%
B20 + TBHQ	-0.9%
B20 + Propyl Gallate	-0.4%
B20 + diphenylamine	+0.7%
B20 + BHA	-4.4%

TBHQ induced a 0.9% reduction in NO<sub>x</sub> emissions when added to B20 at 1000 ppm, but the data from this particular additive had a great deal of scatter. Reductions as high as 8.7% were observed, but other tests showed an increase as great as 5.3%. TBHQ was the only additive that exhibited such erratic behavior.

One possible explanation for this behavior may lie in the storage stability of the antioxidants. Although the antioxidants were stored in a cool, dry place and out of light, they were not stored under inert gas and may have reacted with oxygen, thus reducing their

effectiveness. The possibility of pre-oxidation must be investigated further.

Diphenylamine was notable in that it consistently increased NO<sub>x</sub> emissions, though the increase was small (+0.7%). It is likely that this increase might have been due to the nitrogen present in the additive. Although this increase may not appear significant, it should be considered when selecting an antioxidant for fuel storage stability purposes.

Butylated hydroxyanisole (BHA) was the most effective of the antioxidants studied, giving a 4.4% decrease in measured NO<sub>x</sub> emissions. This decrease is approximately the same as was observed with an identical amount of 2-ethylhexyl nitrate. We conclude that the addition of BHA to the B20 does work to combat the "prompt" NO<sub>x</sub> that is formed during the combustion process.

BHA and TBHQ have similar structures, as shown in Figure 1. Decreases in NO<sub>x</sub> levels observed with TBHQ addition, however, were not repeatable. The similarity in structure of BHA and TBHQ suggests that structure may play a role in determining antioxidant activity and effectiveness in reducing NO<sub>x</sub> emissions.

## Conclusions

The system described in this work was designed for screening additives that may potentially reduce NO<sub>x</sub> emissions from biodiesel. Despite minimal instrumentation, it was possible to observe changes in NO<sub>x</sub> levels with changes in fuel formulations. While more thorough engine testing will be required to confirm the results reported here, the system we used represents a relatively inexpensive approach to examining the effect of fuel additives on NO<sub>x</sub> production by biodiesel fuels.

The use of butylated hydroxyanisole (BHA) should be investigated further as this additive did produce a small but significant decrease in NO<sub>x</sub> emissions. TBHQ also should be investigated. Blends of additives should be investigated to look for synergistic effects.

## References

- (1) Grabowski, M.S.; and McCormick, R.L. *Prog. Energy. Comb. Sci.* **1998**, *24*, 125.
- (2) Choi, C.Y.; and Reitz, R.D. *Fuel*, **1999**, *78*, 1303.
- (3) Song, J.; Cheenkachorn, K.; Want, J.; Perez, J.; Boehman, A.L.; Young, P.J., and Waller, F.J. *Energy and Fuels*, **2002**, *16*, 294.
- (4) Miller, J.A.; and Bowman, C.T. *Prog. Energy Combust. Sci.* **1989**, *15*, 287.
- (5) McCormick, R.L.; Grabowski, M.S.; Alleman, T.L.; Herring, A.M.; and Tyson, K.S. *Environ. Sci. Technol.* **2001**, *35*, 1742
- (6) McCormick, R.L.; Alvarez, J.R.; and Grabowski, M.S. Report NREL/SR-510-31465, **2003**.
- (7) Suppes, G.J.; Goff, M.; Burkhart, M.L.; Bockwinkel, K.; Mason, M.H.; Botts, J.B.; and Heppert, J.A. *Energy and Fuels*, **2001**, *15*, 151.
- (8) Liotta, F.J. *SAE Paper 932767*, **1993**.
- (9) Mittelbach, M.; and Schober, S. *J. Am. Oil Chem. Soc.* **2003**, *80*, 817.

# Functionalization of nickel on 4-aminothiophenol modified glassy carbon electrodes and the enhanced electrochemical activity towards the oxidation of ethanol

Jan Marwan, Ouassim Ghodbane, Eric Lascombe, Gwenaël Chamoulaud, Daniel Bélanger and Mohamed Touaibia

Département de Chimie, Université du Québec à Montréal, Case Postale 8888, succursale Centre-Ville, Montréal (Québec) Canada H3C 3P8

## Introduction

Organized self-assembled monolayers (SAMs) on various solid supports have attracted much attention in recent years and are commonly used to impart desired chemical or physical properties to surfaces. SAM's offer the possibility to control the film structure at the molecular and supramolecular level and therefore to realize the tailoring of the surface properties. Monolayers of organic thiols, especially those formed of alkanethiols, are the most studied self-assembled monolayer system since they offer stability and high degree of organization<sup>1</sup>. Monolayers formed from aromatic thiols, although not that intensively studied, are of considerable interest since they offer together with the properties given by aliphatic thiols the additional advantage of having a high electrical conductivity<sup>2</sup>. Their use as surface modification agents opens up new possibilities to arrange metal particles on modified electrode surfaces with supposedly enhanced electrochemical activity.

It is well-known from the literature that the thiol-containing group of any aliphatic and aromatic compound can be adsorbed onto Pt, Cu and Ag<sup>3</sup>. This might be an interesting approach to the formation and arrangement of metal particles on aryl modified electrode surfaces. Nickel, showing a high affinity to the amine group in nickel amine complexes, is then expected to be functionalized onto the 4-aminothiophenol modified electrode. Nickel has been reported to be a good catalyst for the oxidation of various organic compounds<sup>4</sup>. We have chosen in our studies ethanol as compound with the aim to investigate the electrochemical activity of nickel in this oxidation process.

## Experimental

Glassy carbon electrodes (AIMCOR, Pittsburgh, grade GC-10) were prepared from 3 mm diameter rods embodied into epoxy resin (Hysol, 56C) and were used as working electrodes. Platinum gauze and a Ag/AgCl (saturated KCl) electrode were used as counter and reference electrodes, respectively. All potentials were reported versus the Ag/AgCl reference electrode. The glassy carbon electrode surface was cleaned by polishing with 1  $\mu\text{m}$  and 0.05  $\mu\text{m}$  alumina slurry. After polishing, the electrode was washed with water and ultrasonicated for 5 min in acetonitrile. Electrochemical modification of the glassy carbon electrode was carried out in acetonitrile containing 1 mM aminothiophenol and 0.1 M  $\text{NBu}_4\text{BF}_4$ . The applied potential was 2.0 V for the deposition of 4-aminothiophenol. After the modification, the electrode was thoroughly washed by rinsing in acetonitrile and then in deionized water. A solution containing 97.6 wt% methanol, 2 wt% acetic acid and 0.4 wt% nickel(II)chloride hexahydrate (reduced to Ni zero state by 0.4 M sodium borohydride) has been prepared in which the modified electrode has been soaked for 20 minutes at 45-50 °C to functionalize nickel. After rinsing with deionized water again, electrochemical measurements of the nickel prepared modified electrode were carried out at room temperature (18-23°C) in 1 M NaOH and in further experiments with the addition of ethanol using various concentrations. Before each experiment the

solution was sparged for 10-15 minutes with a stream of highly purified nitrogen to displace dissolved oxygen. Electrochemical measurements were performed in a one-compartment cell using the three-electrode configuration. Cyclic voltammetry was performed using either a potentiostat/galvanostat model M263A (EG&G Princeton Applied Research) or an electrochemical interface SI1287 (Solartron Instruments) interfaced with a PC and the electrochemical set-ups were both controlled with the model DC Corrware (Scribner Associates, version 1.2) software.

## Results and Discussion

Figure 1 shows the typical cyclic voltammetry in 1 M NaOH at 50 mV/s of nickel loaded onto 4-aminothiophenol corresponding to  $1.8 \times 10^{-9}$  mol/cm<sup>2</sup>. Initially the GC electrode surface (0.07 cm<sup>2</sup> electrode area) was modified with 4-aminothiophenol at 2.0 V vs Ag/AgCl for 240s. The voltammetry of nickel is characterized by reasonably well-understood surface reactions corresponding to the formation and stripping of hydroxide films at the metal surface. Starting on the anodic scan we can clearly note in figure 1 the presence of a well-established peak at 0.43 V attributable to the formation of NiOOH, and on the reverse scan the corresponding peak due to the reduction of the anodically formed NiOOH occurs at 0.34 V. More anodically the oxygen evolution arises at the onset potential of 0.55 V. The voltammetric features shown in this figure are comparable to those reported in the literature for ordinary nickel electrodes and dispersed nickel on modified electrode surfaces in basic solution<sup>5</sup>. With the characteristics outlined in this figure we can clearly confirm the presence of nickel functionalized on the modified GC electrode. One could argue that the deposition of nickel might occur onto the glassy carbon surface and this may then be responsible for the voltammetric features given in figure 1. This assumption is rather unlikely since recent studies showed complete blocking of the electrochemistry on the modified electrode when using redoxactive species so that any deposition of nickel onto GC in the presence of 4-aminothiophenol grafted onto the electrode is more to be doubted. This should therefore give strong indication that the presence of nickel in our voltammetry is only due to the surface reactions on the nickel film functionalized on the modified electrode surface.

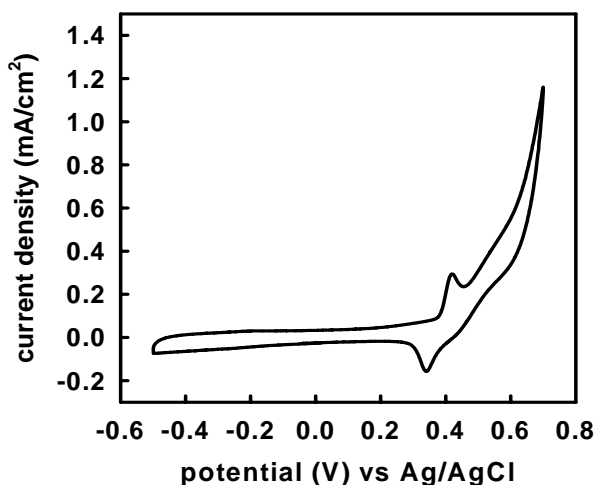
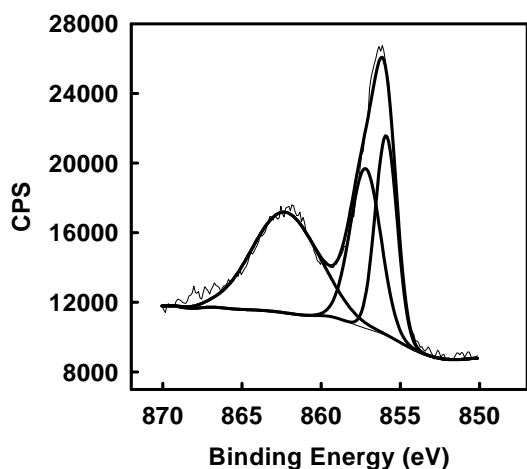


Figure 1. Cyclic voltammetry in 1 M NaOH at 50 mV/s of nickel functionalized onto the 4-aminothiophenol modified GC electrode surface (0.07 cm<sup>2</sup> electrode area). 4-Aminothiophenol as surface modification agent was grafted at 2.0 V vs Ag/AgCl for 240s onto the glassy carbon (GC) electrode.

To give further evidence that nickel is present on the modified GC electrode and to make these studies conclusive, **figure 2** shows the XPS core level spectrum of Ni2p obtained after the functionalization of nickel onto aminothiophenol. We restrict our studies to the Ni2p<sub>3/2</sub> region since this will provide us with sufficient information. Curve fitting of the Ni2p<sub>3/2</sub> gives different Ni species with binding energies of 855.9±0.1 and 857.2±0.1 eV. On the basis of their binding energies these peak values were assigned to Ni(OH)<sub>2</sub> and NiOOH, respectively, with the ratio in area underneath the peak of 0.92. The Ni2p<sub>3/2</sub> spectrum shows at higher binding energies (862±0.2 eV) an intense satellite signal which may be attributed to a multielectron excitation (shake-up peaks). It is relevant to point out that at lower binding energies below 854 eV the XP signal for nickel metal and NiO does not appear in this spectrum. This fact might indicate that Ni is fully covered by an hydroxide layer after its functionalization onto the modified electrode. Further support for this was given by the O1s spectrum. The fact that nickel was shown to be functionalized onto the 4-aminothiophenol electrode surface opens up new possibilities for further investigations in which we were particularly interested in the oxidation of ethanol on nickel.



**Figure 2.** X-ray photoelectron Ni2p core level spectrum for nickel functionalised onto the 4-aminothiophenol modified electrode surface.

Directing our attention towards **figure 3** we notice on following the anodic scan in voltammogram a) a peak at 0.53 V with its corresponding peak on the reverse scan at the same potential. This experimental finding is consistent to that reported in the literature about the ethanol oxidation process on nickel electrodes<sup>6</sup> so that we found our experimental results attributable to this electrochemical process. On continuing the anodic scan we see the start of the oxygen evolution with the onset potential of 0.68 V. Comparing these voltammetric features to those shown in voltammetry b) and c) we hardly note any difference except the fact that higher current densities were obtained with increasing ethanol concentration. This issue is essential, and we certainly want to stress this fact that with increasing the ethanol concentration in figure 3 fast kinetic processes and negligible shift of about a few mV in peak potential for the ethanol oxidation process occur when comparing the voltammetries and thus a clear separation between this process and the oxygen evolution can still be seen even at high ethanol concentrations (5M). These are remarkable features and are clearly in contrast to the results shown in published material on ordinary nickel electrodes<sup>6</sup> and nickel based alloys dispersed on a modified electrode<sup>7</sup>. Here the electrochemical surface reactions are accompanied by an increase in solution resistance near the electrode surface leading then at high ethanol

concentrations to an ohmic drop. Kim and Park<sup>7</sup> showed this behaviour in their work when using Ru-Ni alloys describing that the peak for the ethanol oxidation at higher concentrations (>0.5 M) is rather indistinguishable from the oxygen evolution in the voltammetry. In addition, we want to emphasize the fact that we obtained reasonable current densities for the ethanol oxidation process with a low amount of nickel loaded onto the modified electrode. Comparable electrochemical activity was obtained when using almost 300 fold less quantity of nickel as catalyst material. Running the ethanol oxidation constantly at 0.5 V vs Ag/AgCl in 1 M NaOH using the 4-aminothiophenol modified electrode on which nickel was loaded revealed appreciable current densities (>5mA/cm<sup>2</sup>). With the focus on further improvement we might therefore consider this electrode as one alternative to the Pt based alloy electrodes for the anodic oxidation of ethanol in fuel cells.

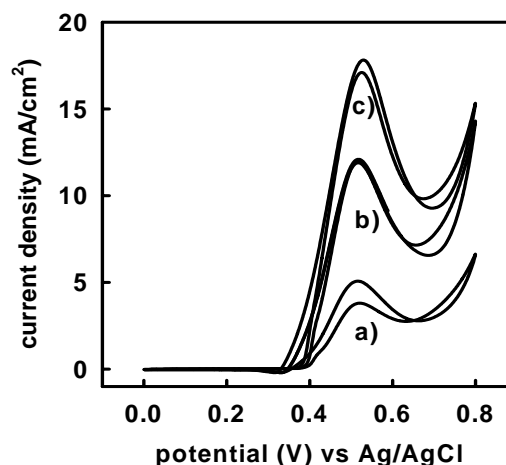


**Figure 3.** Set of cyclic voltammograms at 50 mV/s in 1 M NaOH with increasing concentration of ethanol from 0.5 M a), 2 M b) to 5 M c) of nickel functionalised onto the 4-aminothiophenol modified GC electrode surface. 4-Aminothiophenol as surface modification agent was grafted at 2.0 V vs Ag/AgCl for 240s onto the GC electrode. In this voltammetry the same nickel prepared electrode was used as in figure 1

**Acknowledgment.** We gratefully thank the financial support of the Natural Science and Engineering Research Council of Canada (NSERC).

#### References

- 1) Qu, D.; Morin, M., *J. Electroanal. Chem.* **2002**, 524, 77.
- 2) Hayes, W. A.; Shannon, C., *Langmuir* **1996**, 12, 3688.
- 3) Hubbard, A. T., *Chem. Rev.* **1988**, 88, 633.
- 4) Manandhar, K.; Pletcher, D., *J. Appl. Electrochem.* **1979**, 9, 707.
- 5) Nelson, P. A.; Elliott, J. M.; Attard, G. S.; Owen, J. R., *Chem. Mater.* **2002**, 14, 524.
- 6) Motheo, A. J.; Machado, S. A. S.; Rabelo, F. J. B.; Santos Jr., J. R., *J. Bras. Chem. Soc.* **1994**, 5, 161.
- 7) Kim, J.-W.; Park, S.-M., *J. Electrochem. Soc.* **2003**, 150, E560.

# Kinetics, Characterization and Mechanism for the Selective Dehydration of Ethanol to Diethyl Ether over Solid Acid Catalysts

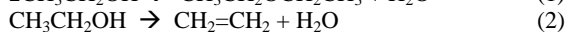
T. Kito-Borsa and S.W. Cowley

Department of Chemistry and Geochemistry  
Colorado School of Mines  
Golden, CO 90401

## Introduction

Ethanol is a clean burning alternative automotive fuel to gasoline<sup>1-2</sup>. However, one serious disadvantage of ethanol is that it has a lower vapor pressure (-3 psia at 38 °C) than winter grade gasoline (~11 psia at 38 °F)<sup>3</sup>. A time-honored standard in the fuel industry mandates that fuels have sufficient vapor pressure to cold-start an automobile at temperatures as low as -30 °C. This is not possible with ethanol. One promising way to solve this problem is to convert a portion of the ethanol into a more volatile compound, such as diethyl ether, on board the vehicle prior to or during the cold-start operation.

The main objective of this study is to develop a catalyst material that exhibits acceptable activity and selectivity for the dehydration of ethanol to diethyl ether (DEE) under the severe operating conditions that exist on board an automobile. Aliphatic alcohols, with exception of methanol, have two modes of dehydration, bimolecular dehydration to produce ethers and intra molecular dehydration to olefins, see equations (1) and (2).



Both dehydration reactions are known to proceed over solid acid catalysts<sup>5</sup>. However, ethylene is undesirable, since it contributes to automotive pollution and catalyst fouling. Diethyl ether formation is thermodynamically favorable over a wide range of temperatures, including the 50-500 °C range commonly employed in catalytic processes. However, the formation of ethylene is also thermodynamically favored and predominates at temperatures above 100 °C. Operating a solid acid catalyst at temperatures below 100 °C results in the selective formation of diethyl ether, but the reaction is kinetically limited and gives rates too slow for an automotive application. In order to overcome this dilemma, a catalyst is needed that can selectively produce diethyl ether at temperatures in excess of 100 °C. In this study, such a catalyst is reported and a possible mechanism for its observed selectivity for diethyl ether production is discussed.

In order to design an on board catalytic dehydration reactor, it is necessary to determine the required fuel properties of a ternary mixture of ethanol, water, and diethyl ether for cold-starting a vehicle. This information is needed in order to determine the % ethanol conversion that is required from an on-board catalytic reactor. This also plays an important role in selecting the appropriate catalyst material and the optimum reaction conditions in our laboratory studies. A significant amount of information has been published regarding ethanol as a fuel<sup>2-3</sup>, but the literature is nearly void of information regarding the diethyl ether assisted cold-starting of a vehicle<sup>5</sup>. Vapor-liquid equilibrium phase diagrams, for ternary mixtures of ethanol, diethyl ether, and water, at various temperatures, have been reported by Kito-Borsa and Cowley<sup>6</sup> using ASPEN Plus software. Their results suggest that ethanol conversions between 40 and 85% at 100% diethyl ether selectivity is required to produce an

acceptable fuel mixture that can cold-start a vehicle at temperatures down to -30 °C without forming two immiscible liquid phases.

Highly acidic ion exchange resins catalyze the dehydration of ethanol almost exclusively to diethyl ether over a temperature range of 80-120 °C<sup>7-8</sup>. Although these materials are highly selective, the narrow temperature range and low reaction rates severely limit their viability for any cold-start application. At temperatures above 120 °C, the particles begin to fuse together causing a dramatic increase in pressure drop through the catalyst bed or a complete blockage of flow<sup>9</sup>. Karpuk and Cowley<sup>10</sup> reported the dehydration of methanol to dimethyl ether (DME) and water occurs readily over fluorinated  $\gamma$ -alumina. Amorphous silica-alumina,  $\gamma$ -alumina, and alumina-phosphoaluminate (APA) also gave good yields. In a review of hydrocarbon formation, Chang<sup>11</sup> discusses the possible mechanisms for DME formation. Depending on the catalyst type, Lewis acid sites, Bronsted acid sites, or both appear to be involved in the methanol dehydration reaction through a complex set of surface reactions. Since all of these catalysts are highly active for methanol dehydration, they may also be suitable for ethanol dehydration as well. The selectivity of these materials for ether versus ethylene production has not been investigated.

## Experimental

The following experimental procedures were used in the evaluation of the catalyst composition and the catalyst performance.

**Catalyst Preparation.** The aluminophosphate-alumina (APA) catalysts were prepared using a conventional coprecipitation method. In general, the APA catalysts were prepared by combining an aqueous solution of aluminum nitrate and orthophosphoric acid with an ammonium hydroxide solution to form a solid hydrogel. The gel was washed with ammonium hydroxide solution, dried at 120 °C for 24 hours, and calcined at 500 °C for 16 hours. The calcined materials were sized to 20/40 mesh. An attempt was made to prepare P/Al ratios of 0.0, 0.1, 0.5, 0.8 and 1.0 by varying the amount of orthophosphoric acid added. The actual P/Al ratios were determined by ICP analysis. The PS-1, PS-2 and PS-3 catalysts were prepared by impregnating 20/40 mesh sized silica gel (Davison Chemical grade 57) with a solution of phosphoric acid. The PA-1, PA-2 and PA3 catalyst was prepared by impregnating 20/40 mesh sized  $\gamma$ -alumina (Norton SA-6273) with a solution of phosphoric acid. The silica-alumina was provided by Davison Chemical (Grade 980-13).

**Catalyst Evaluation.** The catalyst evaluations were carried out under a variety of temperatures in a continuous-flow, fixed bed catalytic reactor, using 1.27 cm o.d. stainless steel tube. Ethanol was injected via syringe pump, then vaporized at 120 °C and mixed with a He (99.9999%) carrier gas. The partial pressure of ethanol in the feed was 0.48, and the space velocity was 2080 cm<sup>3</sup>/g-cat-hr. Approximately, 0.5 g of catalyst was mixed with 1.5 g of quartz chips to insure uniform flow and minimize temperature gradients in the catalyst bed. Each catalyst was tested at 200, 250, and 300 °C for 3 hours at each temperature. The product gas was analyzed by an on-line gas chromatograph (SRI 8610B) using a TC detector and fitted with a 1.5 mm column packed with Porapak Q.

**Catalyst Characterization.** The XRD patterns of the catalysts were collected with a LINT 2000 diffractometer by Rigaku using a Cu K $\alpha$  source at an applied voltage of 40 kV and a current of 150 mA. The radial distribution functions (RDF) of the amorphous APA catalysts were obtained by collecting the x-ray scattering data in the same instrument using a Mo K $\alpha$  source with an applied voltage of 40 kV and a current of 200 mA.

The <sup>27</sup>Al MAS NMR spectra were measured at 130 MHz with a CMX Infinity 500 NMR spectrometer. The sample spin speed was

14 kHz. The spectra were recorded with  $\pi/4$  excitation with a pulse width of 1.0  $\mu$ sec, and a pulse delay of 0.1 second. All of the  $^{27}\text{Al}$  chemical shifts were referenced to a 1 M aqueous solution of aluminum nitrate.

The XPS studies were performed on a Kratos HSi instrument using Al  $K_{\alpha}$  radiation and a band pass of 20 eV.

Temperature programmed desorption (TPD) results were obtained by placing approximately 0.3 g of the catalyst sample in a quartz cell. The sample was pretreated by heating it to 525 °C for 3 hours in a helium flow of 20  $\text{cm}^3/\text{min}$ . Ammonia was adsorbed onto the catalyst sample at 175 °C by flowing a 1:1 volume mixture of anhydrous ammonia and helium through the cell for 30 min. After adsorption was complete, the sample was heated at a rate of 20 °C/min. in flowing helium until a final temperature of 500 °C was reached. The desorbed ammonia was passed through an scrubber containing 20.0 mL of standardized 0.05 N sulfuric acid solution. The total amount of ammonia desorbed was determined by titrating the acid solution with a 0.05 N standard solution of sodium hydroxide. Pyridine was introduced into the helium flow using a saturator maintained at 0 °C. The adsorption period for pyridine was 1 hour.

## Results and Discussion

The catalysts used in this study were selected because they have varying surface densities of Lewis and Brönsted acid sites. Gamma-alumina (GA) has predominantly Lewis acidity, silica-alumina (SA) has both Lewis and strong Brönsted acidity, aluminophosphate-alumina (APA) has both Lewis and weak Brönsted acidity, phosphoric acid on silica (PS) has only Brönsted acidity, and phosphoric acid on  $\gamma$ -alumina (PA) has both Lewis and weak Brönsted acidity. The catalyst compositions are reported in Table 1.

**Table 1. Bulk Composition of Catalysts**

Catalyst	Wt. % $\text{SiO}_2$	Wt. % $\text{Al}_2\text{O}_3$	Wt. % $\text{P}_2\text{O}_5^*$	P/Al Mole Ratio**
GA	0	100		
SA	86.5	13.0		
APA 0.0				0.0
APA 0.1				0.090
APA 0.5				0.488
APA 0.8				0.657
APA 1.0				0.746
PS-1	96.6		3.36	
PS-2	93.9		6.14	
PS-3	86.1		13.9	
PA-1	97.9		2.07	
PA-2	95.5		4.50	
PA-3	90.8		9.20	

\* All of the  $\text{P}_2\text{O}_5$  is present on the surface of the catalyst, and is not distributed throughout the bulk of the sample.

\*\* As determined by ICP analysis.

**Catalyst Evaluation.** The activity and selectivity were calculated using the following equations. Where  $X_E^0$ ,  $X_E$ ,  $X_D$ , and  $X_N$  represent the mole fractions of ethanol in the feed, and ethanol,

$$\% \text{ Activity} = (X_E^0 - X_E) \times 100 \quad (3)$$

$$\% \text{ Selectivity} = X_D / (X_D + X_N) \times 100 \quad (4)$$

dimethyl ether, and ethylene in the product. The catalyst test results are presented in Table 2. A blank run was made using only quartz chips in the catalyst tube. The absence of any ethanol conversion showed that catalytic wall or thermal effects were absent. The conversions for all catalysts were typically less than 10% activity at 200 °C. At temperatures of 250 and 300 °C, only the APA catalysts (0.5-1.0) give activity and selectivity sufficient to cold start a vehicle. A kinetic study was made using the APA 0.5 catalyst. The following rate expression gave the best fit to the data.

$$\text{Rate} = \frac{k'P_E}{(1 + K_E P_E + K_W P_W)} \quad (5)$$

The adsorption constant for water is 436 and that for ethanol is 26.7, which implies that a strong product inhibition by water exists. In summary, the APA catalysts exhibit the desired activity and selectivity for the ethanol dehydration reaction. In order to gain a better understanding of the surface chemistry responsible for this desired result, selected catalysts were analyzed in more detail in order to understand the possible cause of this selectivity.

**Table 2. Catalyst Activity and Selectivity**

Catalyst	250 °		300 °	
	Act.	Sel.	Act.	Sel.
GA	52.5	93.0	83.6	31.4
SA	79.3	71.0	99.2	0
APA 0.0	61.6	93.5	88.1	23.2
APA 0.1	23.3	96.2	73.2	89.3
APA 0.5	54.8	98.0	78.8	87.0
APA 0.8	55.3	98.1	79.5	86.9
APA 1.0	51.5	97.7	78.8	88.5
PS-1	0	-	2.9	54.6
PS-2	2.0	100	4.9	55.4
PS-3	2.4	100	2.8	45.9
PA-1	70.1	92.7	88.6	18.2
PA-2	61.9	94.9	85.4	39.0
PA-3	51.4	97.1	80.9	76.3

**Catalyst Characterization.** Selected catalysts were analyzed by XRD, RDF, NMR, and TPD. Figure 1 shows the XRD patterns for the APA catalysts. The APA 0.0 catalyst contains no aluminophosphate and gives a diffraction pattern similar to the commercial  $\gamma$ -alumina sample (GA). This was the expected result. The addition of even a small amount of phosphate to the structure inhibits the crystallization of the  $\gamma$ -alumina phase. See the XRD pattern for the APA 0.1 catalyst. The addition of more phosphate results in a pattern similar to that of amorphous silica at around 23 degrees  $2\theta$ .

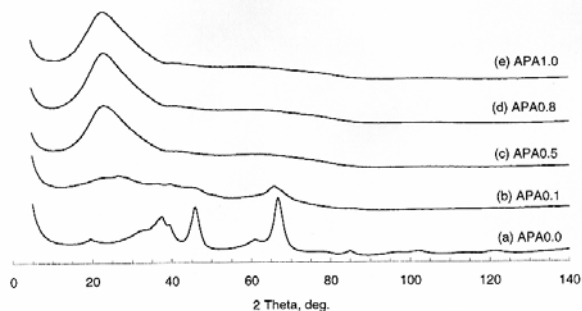


**Figure 1.** XRD patterns for APA 0.0, 0.1, 0.5, 0.8, and 1.0 catalyst samples.

Radial distribution function (RDF) analysis can be used to investigate amorphous materials. A comparison of silica glass, APA 0.1 and APA 1.0 are shown in figure 2. The Al-O (1.74 Å) and P-O (1.74 Å) bond distances are consistent with a tetrahedral configuration, similar to that observed for Si-O (1.61 Å). The variation in the Al-O and P-O bonds is likely responsible for the broader peak observed for the APA 1.0 sample. The APA 0.1 sample gives an Al-O (1.88 Å) bond distance. This value is essentially identical to the Al-O (1.9 Å) bond length reported for an aluminum octahedron<sup>12</sup>. This result suggests that the addition of phosphate forces more aluminum atoms to adopt a tetrahedral configuration.

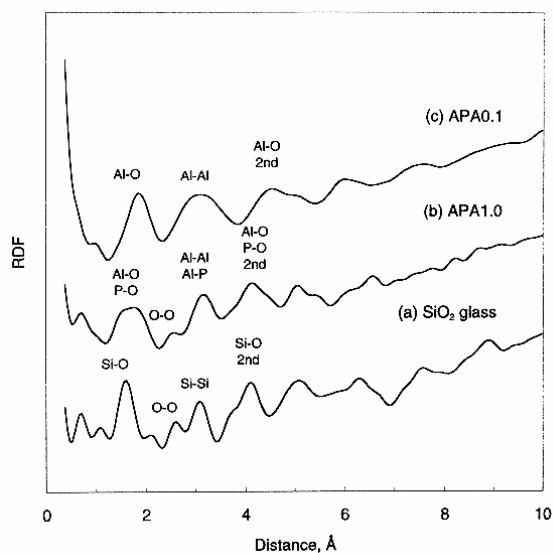


**Figure 2.** RDFs of Silica, APA 0.1 and APA 1.0.

The chemical shifts for the MAS NMR spectra for the <sup>27</sup>Al atoms in samples of GA, APA 0.1, APA 1.0, PA-1, and PA-3 are given in table 3. For the GA sample, the <sup>27</sup>Al atoms are present in 4-coordinate (tetrahedral) sites at 67.4 ppm and 6-coordinate (octahedral) sites at 9.1 ppm, see figure 3. The observed octahedral to tetrahedral ratio of 2.0 : 0.9 is typical for  $\gamma$ -alumina<sup>13</sup>. As phosphate is added to the structure, a new 5-coordinate site appears at 34.0 ppm, apparently at the expense of tetrahedral sites. The

**Table 3. Chemical Shifts for NMR Spectra of <sup>27</sup>Al.**

Catalyst	<sup>27</sup> Al MAS NMR Chemical Shift (ppm)		
	4-coord.	5-coord.	6-coord.
GA	67.4	0	9.1
APA 0.1	71.3	34.0	5.2
APA 1.0	44.1	17.6	-9.6
PA-1	67.4	0	8.3
PA-3	69.0	0	9.9

APA 1.0 sample shows a dramatic change in the NMR spectra, with all three <sup>27</sup>Al peaks being shifted to the right, and a significant increase in the 4-coordinate species. This is in agreement with the RDF data. It is likely that this new species plays a role in making the APA catalysts more selective for diethyl ether production. The PA-1 and PA-3 samples gave NMR spectra very similar in peak area and chemical shifts to that for  $\gamma$ -alumina. This is expected since the phosphate is only located at the surface and the preponderance of the NMR signal comes from the  $\gamma$ -alumina support.

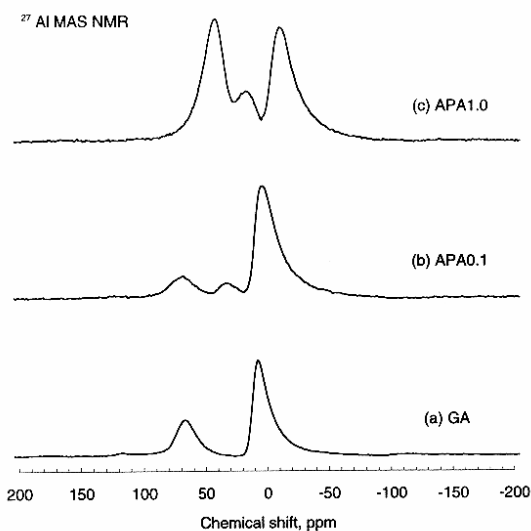


**Figure 3.** <sup>27</sup>Al MAS NMR Spectra of GA, APA 0.1, and APA 1.0 catalyst samples.

XPS analysis of the APA samples was done to determine if there was a direct correlation between the surface and bulk phosphorus to aluminum (P:Al) mole ratio. No enrichment of phosphorus on the surface of the APA samples was observed.

Ammonia and pyridine TPD studies provide information about the relative amounts of Lewis and Brønsted acid sites on the catalyst surfaces. Ammonia is known to adsorb onto both Lewis and Brønsted acid sites, while pyridine adsorbs only onto Lewis acid sites. Since Brønsted sites of  $\gamma$ -alumina, Al-OH, are too weak to protonate pyridine, Lewis acidity is thought to be exclusively responsible for the observed acidity for  $\gamma$ -alumina<sup>14</sup>. Silica is known to have very little acidity. Table 4 gives the TPD results for the desorption of ammonia and pyridine from our catalyst samples.

**Table 4. Relative amounts of ammonia and pyridine desorption from catalyst samples.**

Catalyst Sample	Ammonia Desorbed	Pyridine Desorbed	Pyridine to Ammonia Des. Ratio
GA	0.89	1.69	1.91
SA	0.55	0.48	0.86
APA 0.0	0.76	1.27	1.67
APA 0.1	0.55	0.74	1.36
APA 0.5	2.12	1.10	0.52
APA 0.8	2.59	0.86	0.33
APA 1.0	3.04	0.74	0.24
Silica	0.04	0.03	0.57
PS-1	0.34	0.29	0.86
PS-3	2.04	0.74	0.36
PA-1	0.91	1.60	1.77
PA-2	0.88	1.52	1.73
PA-3	0.99	1.46	1.47

A decrease in the ratio of pyridine to ammonia desorption suggests a decrease in the population of Lewis acid sites. The pyridine to ammonia ratio decreases for the APA catalysts as the phosphate

content increases. Considering these observations, it is apparent that the addition of phosphate decreases the surface concentration of Lewis acid sites. This has important implications with respect to the surface dehydration mechanism. It is proposed that the dehydration of ethanol to ethylene requires two adjacent Lewis acid sites or strong Brønsted acid sites. The APA catalysts dilute the surface concentration of Lewis acid sites without adding strong Brønsted acid sites. The dehydration of ethanol to diethyl ether requires only a single Lewis acid site.

### Conclusions

The unique acidic properties of the aluminophosphate-alumina catalysts make them highly selective for the dehydration of ethanol to diethyl ether at elevated temperatures (200-300 °C).

**Acknowledgement.** This work was funded by DOE and NREL. Catalyst support samples were provided gratis of Grace (Davison Division) and Norton Chemical Companies.

### References

- (1) Cook, G. "A Question of Balance", *NREL in Review: Science and Technology*, **1994**, 16 (2, summer), pp. 2-5.
- (2) Egebäck, K. E., Petersson, L. J., and Westerholm, R., XI International Symposium on Alcohol Fuels proceedings Vol. 1, 1996, pp. 750-761, Sun City, South Africa.
- (3) Barber, E., Quissek, F., and Hulak, K., IX International Symposium on Alcohol Fuels proceedings Vol. 2, 1991, pp. 566-573, Florence, Italy.
- (4) De Boer, J. H., Fahim, R. B., Linsen, B. G., Visseren, W. J., De Vleeschauwer, W. F. N. M. *J. Catal.* **1967**, 7, 163-172.
- (5) Nagai, Y. and Ishii, N. *J. Soc. Chem. Ind. Japan*, **1935**, 38, 8-12.
- (6) Kito-Borsa, T., Pacas, D. A., Salim, S. and Cowley, S. W. *Ind. & Eng. Chem. Res.*, **1998**, 37(8), 3366-3374.
- (7) Apecetche, M. A., and Cunningham, R.E., *Lat. Am. J. Chem. Eng. Appl. Chem.* **1976**, 6, 91-103.
- (8) Gates, B. C., and Johanson, L. N. *J. Catal.* **1969**, 14, 69-76.
- (9) Kito, T., Wittayakun, J., Pacus, D., Selim, S., and Cowley, S. W., XI International Symposium on Alcohol Fuels proceedings Vol. 1, 1996, pp. 166-177, Sun City, South Africa.
- (10) Karpuk, M. and Cowley, S. W. International Fuels and Lubricants Meeting and Exposition, Portland, Oregon, 1988, October 10-13, *SAE Technical Paper Series*, 881678.
- (11) Chang, C. D., *Catal. Rev. Sci. Eng.*, **1983**, 25, 36-48.
- (12) Shannon, R. D. and Prewitt, C. T., *Acta Cryst.* **1969**, B25, 925-946.
- (13) Müller, D., Gessener, W., Behrens, H. J., and Scheler, G. *Chem. Phys. Lett.* **1981**, 79, 59-62.
- (14) Peri, J. B. *Discuss. Faraday Soc.* **1971**, 52, 55-65.

# EFFECTS OF NITROGEN CHEMISTRY ON CHAR FORMATION FROM BIOMASS

Robert J. Evans, Mark R. Nimlos, Luc Moens

National Bioenergy Center  
National Renewable Energy Laboratory  
Golden, Colorado 80401

## Introduction

The fate of nitrogen during pyrolysis or combustion is an important consideration in the utilization of biomass. Nitrogen oxide emissions from biomass combustion are thought to arise primarily from fuel-bound nitrogen<sup>1</sup> and an understanding of the chemical transformations involving nitrogen may lead to improvements in these emissions. An important source of nitrogen in biomass is proteins and amino acids, which can react catalytically with the carbohydrates by reactions generally characterized as Maillard chemistry<sup>2</sup>. This chemistry produces complex mixtures of products and has been the subject of numerous studies. However, less is known about the role that this chemistry plays in the formation of char. The partitioning of nitrogen into char or gas phase products will be critical towards determining the routes for converting nitrogen from biopolymers into NO<sub>x</sub> emissions.

We have studied reactions of amino acids with carbohydrates and how these reactions affect the composition of the resulting char. We have used Molecular Beam Mass Spectrometry (MBMS) to characterize the gaseous emissions from the pyrolysis of model mixtures of amino acids with carbohydrates. The remaining char has been characterized using elemental analysis and reflectance FTIR spectroscopy.

Of particular interest in the char formation are effects due to the Maillard chemistry involving proline. We have shown that proline is more reactive in Maillard chemistry than other amino acids<sup>3</sup>, which is consistent with literature reports of proline as a catalyst for asymmetric aldol condensations<sup>4-6</sup>. In particular, we would like to investigate how proline affects the maturation of char.

## Experimental Techniques

Experiments were conducted by sequentially heating samples of model compounds or biopolymers in flowing helium. Gas phase products were measured directly using an MBMS, and the remaining solid materials were retained for further analysis. Samples (100 mg to 400 mg) were placed in a quartz boat and slid into a heated tubular reactor. The furnace was set so that sliding the sample further into the reactor produces higher temperatures. Sequential heating experiments were conducted by sliding the sample into a fixed temperature region (as determined by a thermocouple attached to the boat) and holding for five minutes. A subsequent heating was conducted by sliding the material further into the reactor and holding it at that higher temperature for five minutes.

## Results and Discussion

Figure 1 shows integrated mass spectra for staged heating experiments using proline mixed with a carbohydrate matrix composed of glucose, cellulose and pectin (Pro:Glu:Cell:Pect = 1:1:2:2). This mixture was used because the glucose will react vigorously with the glucose and the cellulose/pectin mixture produces a significant amount of char. In these experiments, the samples are heated to 550 °C directly (bottom spectrum) or sequentially (top two spectra). In the spectrum on the top, the sample was heated to 170 °C for 5 min. then to 350 °C for 5 min. before being heated to 550 °C. In the middle spectrum the sample was heated to 350 °C before being

heated to 550 °C. The mass spectra in this figure are obtained by integrating over the pulse that occurs during the last temperature of each given sequence.

The intensity of the high m/z peaks are shown in the insets and the scales for these are on the right side of the plots. As can be seen, there are characteristic clusters of peaks in the high m/z portion of these spectra. For instance, there are clusters around m/z = 200, 214, 227 and 242. These spectral clusters are also observed for other amino acids but are not as prominent as for proline. Furthermore, the location of these clusters seems to be dependent upon the amino acid but not the type of carbohydrate used. These peaks appear to be associated with Maillard reactions between proline and the carbohydrates and probably result from secondary reactions. As can be seen from these spectra, the formation of these high m/z clusters of peaks is enhanced when the sample is not thermally pretreated. They are more intense in the bottom spectrum than in the middle spectrum and more intense in the middle spectrum than in the top spectrum. This suggests that low temperature reactions of the proline with the carbohydrates tend to decrease the formation of these secondary Maillard products.

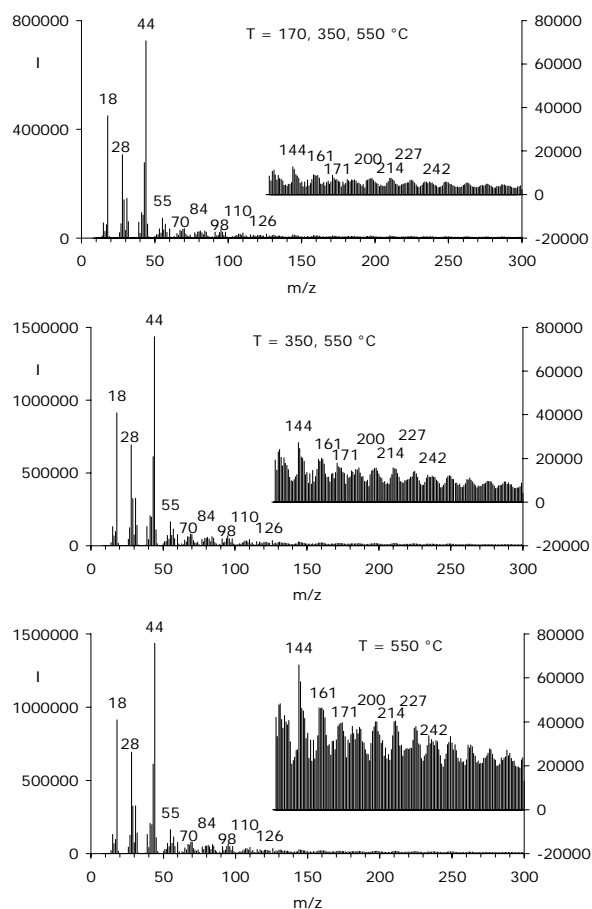


**Figure 1.** Mass spectra from the staged heating of proline mixed with a matrix of glucose, cellulose and pectin. These spectra have been averaged over triplicate experiments.

The infrared spectra of the char also shows interesting changes in the solid that result from Maillard reactions. Fig. 2 shows a plot of

the FTIR spectra of the char from the pyrolysis of our carbohydrate matrix without proline. The lower spectrum is of the unheated matrix. The peaks at 3300  $\text{cm}^{-1}$  (O-H stretch), 2890  $\text{cm}^{-1}$  (C-H stretch), 1330  $\text{cm}^{-1}$  (C-H bend) and 1050  $\text{cm}^{-1}$  (C-O stretch) are characteristic of carbohydrates. At moderate pyrolysis temperatures (170  $^{\circ}\text{C}$  and 350  $^{\circ}\text{C}$ ) carbonyl peaks are formed (1750  $\text{cm}^{-1}$  and 1630  $\text{cm}^{-1}$ , C=O stretch). At 550  $^{\circ}\text{C}$  peaks arising from aromatic groups are seen at 3040  $\text{cm}^{-1}$  (C-H stretch), 1590 and 1436  $\text{cm}^{-1}$  (C-C stretch), 1230  $\text{cm}^{-1}$  (C-H in-plane bend) and 815  $\text{cm}^{-1}$  (C-H out-of-plane bend).

Similar peaks are seen in the char FTIR spectra shown for proline (Fig. 3) mixed with the carbohydrate matrix. However, the presence of the proline leads to maturation of the char at lower temperatures. For neat matrix experiments there is still significant intensity for the carbohydrate peaks at 350  $^{\circ}\text{C}$ , while in the presence of proline, these peaks are essentially gone at 350  $^{\circ}\text{C}$ . For the mixture including proline the carbonyl peaks form at 170  $^{\circ}\text{C}$  but disappear at 350  $^{\circ}\text{C}$ , where they are replaced by aromatic peaks. This again shows the ability of proline to accelerate the char maturation process. Other amino acid can also accelerate the formation of aromatic groups in char but not to the extent that occurs with proline.

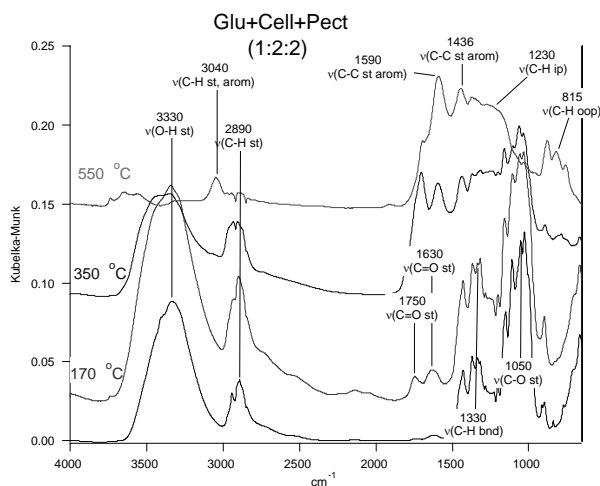


**Figure 2.** Reflectance FTIR spectra of carbohydrate matrix heated to different temps.

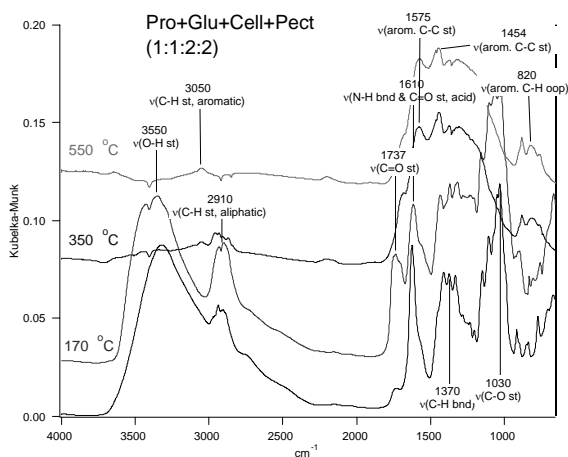


**Figure 3.** Reflectance FTIR spectra of char from pyrolysis of proline + matrix.

Measurement of char yields from the sequential pyrolysis experiments and elemental analysis of the remaining solid material allow a determination of the partitioning of nitrogen for the solid and gas phase. The plot in Fig. 4 shows this partitioning for sequentially heating a mixture of proline and the carbohydrate matrix to 170 $^{\circ}\text{C}$ , 350  $^{\circ}\text{C}$  and 550 $^{\circ}\text{C}$ . This plot shows that the nitrogen has a tendency to stay in the char.

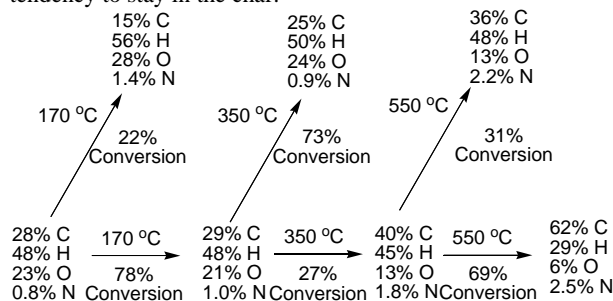


**Figure 4.** Partitioning of elements during sequential heating of proline mixed with the carbohydrate matrix (Glu+Cell+Pect). The composition in the lower left is for the starting material and the values along the bottom are for the char after heating. The values at the top are for the gas phase after heating.

### Conclusions

The conclusions of this work are that proline can drastically change the rate of formation of mature char (highly aromatized) through its vigorous reaction with carbohydrates. Further, this Maillard chemistry appears to leave significant amounts of the nitrogen in the char.

**Acknowledgment.** We would like to acknowledge the support of Philip Morris USA, and stimulating discussions with Geoffrey Chan and Mohammad R. Hajaligol.

### References

1. Brink, A., P. Kilpinen, and M. Hupa, *Energy Fuels*, 2001. 15(5): 1094.
2. T. P. Labuza, G.A.R., V. M. Monnier, J. O'Brien, J. W. Baynes, ed. *Maillard Reactions in Chemistry, Food and Health*. 1994, Royal Society of Chemistry: Cambridge.
3. Moens, L; Evans, R. J; Looker, M. J.; Nimlos, M. R. *Fuel*, In Press.
4. Movassaghi, M. and E.N. Jacobsen, *Science*, 2002. 298(5600): 1904.
5. Sakthivel, K., W. Notz, T. Bui, and C.F. Barbas, *J. Am. Chem. Soc.*, 2001. 123(22):5260.
6. List, B., R.A. Lerner, and C.F. Barbas, *J. Am. Chem. Soc.*, 2000. 122(10): 2395.

# NMR STUDY OF THE TRANSFORMATIONS IN PECTIN AND CELLULOSE (WITH 10% N-15 PROLINE) DURING PYROLYSIS

R. J. Pugmire, M. S. Solum, Z. Ma,  
Y. J. Jiang, J. B. Wooten\*

Department of Chemical and Fuels Engineering, University of Utah, Salt Lake City, Utah 84112 and Philip Morris USA Research Center, \*P.O. Box 26583, Richmond, Virginia 23261

## Introduction

In preparation for the analysis of tars made from a tobacco plant grown from N-15 enriched nutrients several chars made from pectin and cellulose (with 10% by weight of N-15 enriched proline added) have been studied by C-13 and N-15 NMR and ESR methods. The carbon skeletal structure was analyzed in terms of the previously described structural and lattice parameters.<sup>1,2</sup> Only a few of the highest temperature chars (550 and 600 °C) start to show a small amount of graphite like structures.<sup>3</sup> The spin lattice relaxation time in both the laboratory and rotating frame were measured for all samples and showed correlation with the carbonization of the samples.

## Experimental

All C-13 NMR spectra were run on a Chemagnetics CMX-100 spectrometer operating at a carbon frequency of 25.152 MHz and using a 7.5 mm probe with a ceramic housing for reduced carbon background. The proton decoupling power was 62.5 kHz. The spinning speed was locked to 4.1 kHz. Chemical shift ranges used in references 1 and 2 were modified to somewhat account for the overlap of the aromatic region with the anomeric carbon in carbohydrates in some of the samples. The contact time chosen for the dipolar dephasing experiments was five times the longest  $T_{CH}$  as measured in variable contact time experiments.

Nitrogen-15 spectra were run on a Chemagnetics CMX-200 spectrometer also with a 7.5 mm probe. This field was chosen, instead of the higher S/N spectrometer operating at 400 MHz, so that the formation of pyridinic type nitrogens with large chemical shift anisotropies could be more accurately followed.<sup>3</sup>

All chars were prepared at Philip Morris and heated to temperatures of 150 to 600 °C.

## Results and Discussion

Carbon-13 CPMAS spectra of some pectin chars are shown in Figure 1. The pectin resonances are the larger broader resonances at about: 171 ppm for the carboxyl carbon, 101 ppm for the anomeric carbon, 70 ppm for carbons next to one oxygen and 54 ppm for the methoxy group. The five resonances from proline are the smaller sharper lines. As can be seen in the spectrum from the sample heated to 150 °C proline is the first to react. A small amount of aromatic and carbonyl carbons have been produced where there were none in the original mixture. Also the aliphatic part of the spectrum has become broad in the region where the sharp proline resonances were before. At 250 °C most of the pectin has also reacted and the spectrum looks like a lignite coal. A large amount of aromatic carbons have been formed but the sample still retains a wide range of oxygen functional groups: carbonyls, carboxyls, phenolics and oxygenated aliphatic carbons. There may still be a small amount of anomeric carbons under the aromatic band at about 105 ppm. These may be able to be separated from the

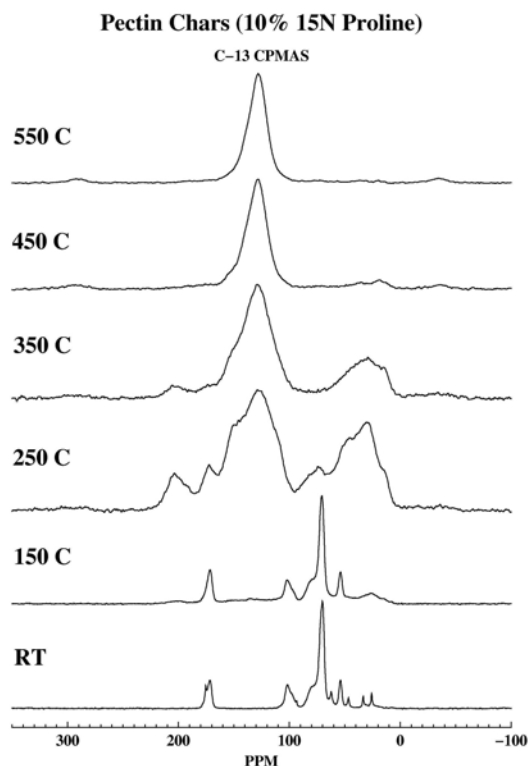


Figure 1. C-13 CPMAS spectra of the pectin and proline mixture heated to the listed temperatures.

aromatic carbon by a csa type filtering experiment.<sup>5</sup> At 350 °C the original material has mostly reacted and the oxygen functional groups have greatly decreased along with some aliphatic material. As the temperature is increased further the samples become more and more aromatic. At 550 °C the aromaticity is 0.95. The average aromatic cluster size is estimated to be about 9 in the 150 °C sample where the aromatic material first starts to appear and progressively increases to about 19 carbons in the 550 °C sample.

Some important NMR relaxation parameters for the pectin/proline samples are presented in Table 1. One can see that after some scatter in the starting sample and the 150 °C sample that the  $T_1^H$  values decrease as the temperature that the sample was heated increased. Others have seen this relaxation time go through a minimum and then increase when the electron spin exchange rate changes and the relaxation is not proportional to the number of static unpaired electrons.<sup>6</sup> The spin-lattice relaxation in the rotating frame,  $T_{1\rho}^H$ , also decreases as the temperature is increased, reaches a minimum at 450 °C, and then starts to increase for the 550 °C sample. This is a common occurrence that has been seen in other pyrolysis series.<sup>2,6</sup>

**Table 1. NMR Parameters from Pectin Chars.**

Sample	$T_1^H$ (s)	$T_{1\rho}^H$ (ms)	$T_L$ (ms)
RT	0.188(76%) 4.97(24%)	3.8 (line 2)	--
150 °C	0.729(94%) 10.9(6%)	6.0(whole spectrum)	0.38
250 °C	0.271	5.4	0.67
350 °C	0.131	2.7	0.79
450 °C	0.027	2.1	1.3
550 °C	0.017	8.4	1.7

The last column in Table 1 is the Lorentzian (exponential) time constant from a dipolar dephasing experiment. This time constant represents dephasing from protons that are not directly attached to aromatic carbons. The dipolar dephasing<sup>7</sup> experiment used here was sequence C from reference 7 that does not include dephasing from chemical shift anisotropy. As one can see as the temperature increases the time constant  $T_L$  gets larger as there are fewer protons or the protons are farther away from the nonprotonated aromatic carbons.

### Conclusions

This preprint shows that NMR can be used to quantify the changes in the structure in a pectin/proline mixture heated to various temperatures. Additional work is currently under way to study the nitrogen incorporation in the various chars and to measure the unpaired electron spin concentration and see how it correlates to the various NMR relaxation time constants. Additional samples heated between 150 °C and 250 °C are currently being examined because this is the temperature range where the largest amount of structural modification seems to occur.

**Acknowledgement.** This work was supported by Phillip Morris, USA.

### References

1. Solum, M. S., Pugmire, R. J., Grant, D. M., *Energy & Fuels*, **1989**, 3, 187.
2. Solum, M. S., Sarofim, A. F., Pugmire, R. J., Fletcher, T. H., Zhang, H., *Energy & Fuels*, **2001**, 15, 961.
3. Jiang, Y. J., Solum, M. S., Pugmire, R. J., Grant, D. M., *Energy & Fuels*, **2002**, 16, 1296.
4. Kelemen, S. R., Afeworki, M., Gorbaty, M., Kwiatek, P. J., Solum, M. S., Hu, J. Z., Pugmire, R. J., *Energy & Fuels*, **2002**, 16, 1507.
5. Mao, J.-D., Schmidt-Rohr, K., *Solid State NMR*, **2004**, in press.
6. Wind, R. A., Li, L., Maciel, G. E., Wooten, J. B., *Appl. Magn. Reson.*, **1993**, 5, 161.
7. Newman, R. H., *J. Magn. Reson.*, **1992**, 96, 370.

# PROBING THE PYROLYSIS OF METAL DOPED CELLULOSE CHARs AT DIFFERENT POINTS ALONG THE REACTION COORDINATE

Andrew M. Herring, J. Thomas McKinnon, Joshua G. Lee, Bryan D. McCloskey, Ryan A. Pavelka, Matthew S. Kirchner, and Dimitri R. Dounas-Frazer.

Department of Chemical Engineering  
Colorado School of Mines  
Golden, CO 80401-1887

## Introduction

Cellulose is a major component of biomass, along with hemicellulose and lignin, and is a useful model for thermo-chemical conversion of biomass. The conversion of biomass via pyrolysis has important applications in the development of new renewable chemicals and bio-carbons, as well as combustion processes leading to combined heat and power, forest fires and cigarette smoking. The process of cellulose and cellulose char pyrolysis is still not fully understood despite rapid progress in the last couple of decades.<sup>1-3</sup> The influence of metal salts on charring and subsequent pyrolysis has long been known to alter the chemistry of these processes.<sup>1,4</sup> Metal cations occur naturally in biomass particularly in the hemicellulose, they may also be added to the growing plant in the form of fertilizer. In general inorganic materials in the form of ash are considered a problem that must be mitigated against in the pyrolysis and combustion of biomass.<sup>5</sup> However, metal cations may be deliberately added to the biomass to alter its pyrolysis chemistry in a favorable way to reduce the formation of polycyclic hydrocarbons, PAH, or in the synthesis of new bio-carbons.<sup>6</sup>

In order to more fully understand the effect of metal doping on cellulose pyrolysis chemistry we have doped Avicel cellulose with a series of mono- and di-valent cations. Both main group and transition metals were chosen in order to probe both the effects of promoting ionic pathways and possible catalytic pathways in the charring and pyrolysis chemistry. We chose to dope cellulose with metal acetates as not only is the acetate anion relatively inert but all of these metal acetates decompose below the charring temperature of 375 °C. The chars were characterized primarily by DRIFTS and NMR. The char structure and pyrolysis chemistry at very short times, several ms, was studied by laser pyrolysis molecular beam mass spectroscopy, LP-MBMS.<sup>7,8</sup> We also sampled the product gases and trapped the free radicals produced using cold and chemical trapping at slightly longer times, several 100 ms.

## Experimental

Avicel cellulose (5 g) was doped at 1mol% with sodium, potassium, magnesium, calcium, palladium, copper and zinc acetates by the incipient wetness technique using aqueous solutions of the as received metal acetates. The doped cellulose samples were dried in an oven at 115 °C overnight pressed into a 1" diameter pellet at 10,000 psi in a Carver press and charred under Ar(g) at 375 °C for ½ h.

For the DRIFTS experiments the chars were ground in air and placed in a Harrick Scientific, heatable variable atmosphere chamber in a Harrick Scientific Praying Mantis Diffuse Reflectance attachment. The chars were heated under dry He(g) for 10 mins at 400 °C and then cooled to room temperature at which point the DRIFTS was recorded using a Thermo-Nicolet Nexus 670 FT-IR spectrometer equipped with a N<sub>2</sub>(l) cooled MCT detector. The data was treated with a Kubelka-Munk transformation to enable its quantitative interpretation.

The details of the LP-MBMS experiment have been described previously.<sup>8</sup> After cooling, the metal doped cellulose char samples were transferred under inert gas to a He(g) filled chamber. LP-MBMS experiment performed at 6.5 W for 2 s. The first 0.25 s data corresponding to a temperature between 900 and 1000 °C is reported here.

For the cold-trapping experiments the charred pellet was mounted in the center of a N<sub>2</sub>(l) cooled brass collection cup, ca. 2 mm from the cold surface. The brass collection cup had been previously coated with Diphenyldisulfide to which a known quantity of chlorobenzene had been added as an internal standard. The charred pellet was irradiated with the CO<sub>2</sub> at 13 W whilst being spun through one revolution. After the experiment, the cold trap is washed with methylene chloride. The methylene chloride extract is filtered and concentrated by evaporation. The concentrated extract is then injected onto a capillary GC column and the species identified using a MSD. We cannot currently observe species smaller than toluene or benzothiophene, because of the elution of the large solvent peak

## Results and Discussion

The DRIFTS of the reheated and dried samples are shown in Figure 1. All of the samples show the same basic spectral features at the following approximate locations, a broad ν(OH) reaching a maximum at 3400 cm<sup>-1</sup>, sharper aliphatic and aromatic ν(CH) at 2900 cm<sup>-1</sup>, a ν(C=O) at 1750 cm<sup>-1</sup>, an aromatic ν(C=C) at 1650 cm<sup>-1</sup>, a complex fingerprint region and two weaker aromatic γ(CH) bands at 850 cm<sup>-1</sup>. Clearly metal doping has a profound effect on the residual char especially in terms of the ratio of OH and carbonyl groups to hydrocarbon. The palladium doped char has by far the most OH remaining in the structure whereas sodium and potassium have the least. The copper doped char has the highest ratio of carbonyl to aromatic hydrocarbon.

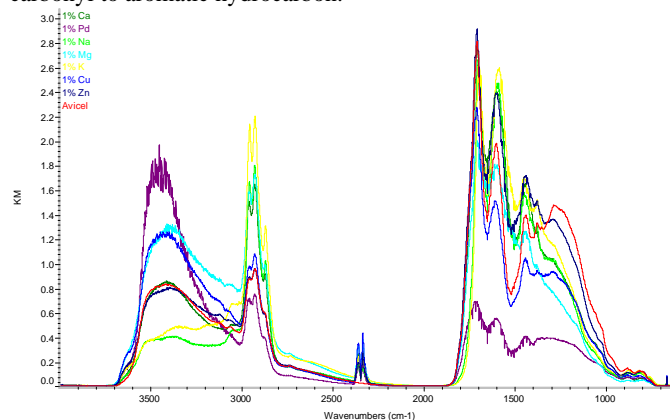


**Figure 1.** DRIFTS of cellulose and 1 wt% doped cellulose ½ h 375 °C chars after heating to 400 °C under He(g).

Solid state MAS <sup>13</sup>C NMR, not shown, also shows similar profound differences between the doped char samples. The zinc doped char appears similar to the undoped char, whereas most of the other chars appear very different or appear to have charred less.

The LP-MBMS experiment may be regarded as a snapshot of the initial reactive cloud of molecules evolved from the pyrolyzing char surface. The primary radical that we have proposed to evolve with these species is propargyl.<sup>7,8</sup> When Avicel cellulose is doped by wt% of metal acetate and charred the amount of CO<sub>2</sub> produced during pyrolysis is proportional to the molar amount of metal originally doped. This implies that one of the basic reactions of the metal in the char is to stoichiometrically oxidize the adjacent char. All metal doped chars produce slightly more toluene than the

undoped cellulose but palladium doped char produces a much larger quantity of this species than any other char during pyrolysis. The relative intensities of PAH species relative to  $m/z$  202, pyrene are shown in Figure 2. It can be seen that whilst the initial ratios of the species produced are altered no distinct pattern emerges. All the chars produce more  $m/z$  215, potassium doped more so. Universal suppression of PAH is only seen for the larger  $m/z$  263 and 304. Most of the metals actually increase the initial amount of  $m/z$  252, benzo-*a*-pyrene.

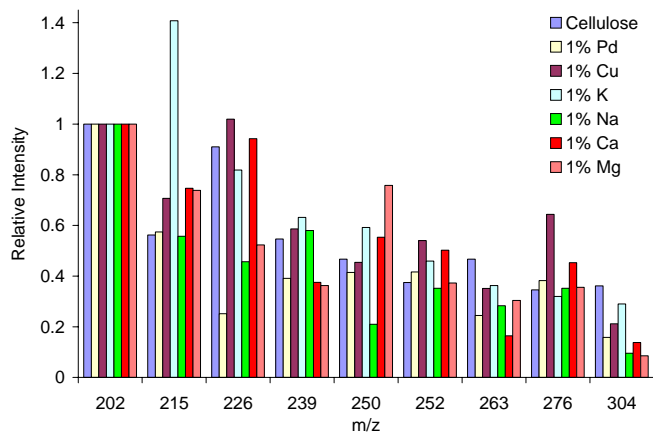


**Figure 2.** Relative intensities vs.  $m/z$  202, pyrene, of selective masses of cellulose and 1 wt% doped cellulose.

In the chemical/cold trap experiment radicals are trapped as their phenylsulfide adducts, Figure 3. No propargyl radical is observed in the cold trap experiment as presumably the reaction is being sampled further along the reaction coordinate. The dominant reactive species observed from cellulose char is the hydrogen radical, together with methyl, phenyl, and phenylacetylene (trapped as benzothiophene) radicals. Only calcium doping cause the amount of these trapped radicals to increase. Palladium and calcium create the observance of methyl naphthalene radical. All the other metals in general suppress the formation of radicals consistent with a more ionic char decomposition pathway during pyrolysis.

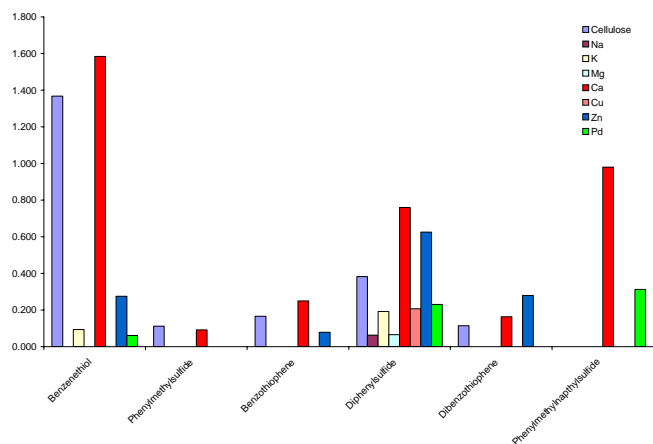


**Figure 3.** Relative abundances of PhS trapped reactive intermediates from the 13 W laser pyrolysis of  $\frac{1}{2}$  h 375 °C Avicel cellulose char and 1 mol% metal acetate doped Avicel cellulose char.

In addition to the chemically trapped radicals we also observe the PAH formed at this point of the reaction. The slate of aromatic and PAH species observed for the undoped cellulose char are shown

in Figure 4. Toluene, naphthalene and acenaphthalene are the dominant products. In addition to the hydrocarbon species we also observe a number of *O*-aromatic molecules. PAH as big as benzofluoranthene are easily observed. The ratio of these products changes with metal doping and further analysis of this data should provide insight in to some interesting trends.

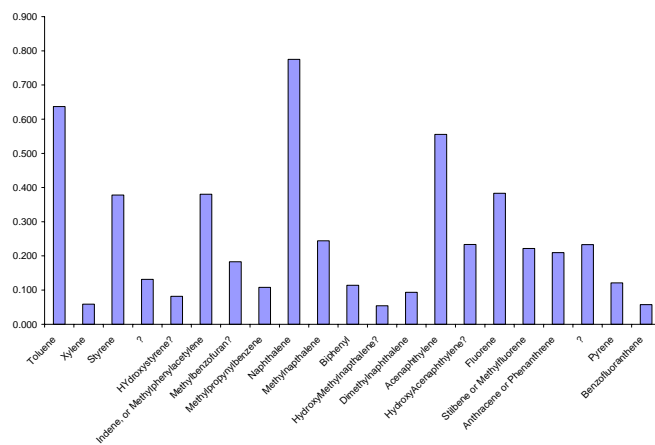


**Figure 4.** PAH observed from the 13 W laser pyrolysis of  $\frac{1}{2}$  h 375 °C Avicel cellulose char.

### Conclusions

Obviously the fact that the PAH are still in existence with radicals in the LP-MBMS and cold trap experiment suggest that we are not yet observing the final slate of reaction products. We hope to be able to correlate the LP-MBMS data with the cold trapped data with conventional tube furnace data in order to build a complete picture of the reaction pathways involved in the pyrolysis evolved reacting volatile plume.

**Acknowledgement.** We would like to thank Philip Morris, USA, for support.

### References

- (1) Evans, R. J.; Milne, T. A. *Energy & Fuels* **1987**, *1*, 123.
- (2) Antal Jr., M. J.; Grnli, M. *Ind. Eng. Chem. Res.* **2003**, *42*, 1619
- (3) Shafizadeh, F. *Journal of Analytical and Applied Pyrolysis* **1982**, *3*, 283.
- (4) Sekiguchi, Y.; Shafizadeh, F. *Combustion and Flame* **1984**, *29*, 1267.
- (5) Davidsson, K. O.; Stojkova, B. J.; Pettersson, J. B. C. *Energy Fuels* **2002**, *16*, 1033
- (6) Herring, A. M.; McKinnon, J. T.; McCloskey, B. D.; Filley, J.; Gneshin, K. W.; Pavelka, R. A.; Kleebe, H.-J.; Aldrich, D. J. *Journal of the American Chemical Society* **2003**, *125*, 9916
- (7) Herring, A. M.; Thomas McKinnon, J.; Gneshin, K. W.; Pavelka, R.; Petrick, D. E.; McCloskey, B. D.; Filley, J. *Fuel* **2004**, *In Press, Corrected Proof*.
- (8) Herring, A. M.; McKinnon, J. T.; Petrick, D. E.; Gneshin, K. W.; Filley, J.; McCloskey, B. D. *Journal of Analytical and Applied Pyrolysis* **2003**, *66*, 165.

# QUANTUM MECHANICAL MODELING OF THE DECOMPOSITION OF SUGARS DURING ACID HYDROLYSIS OF BIOMASS

Mark R. Nimlos, Xianghong Qian, David K. Johnson, Michael E. Himmel

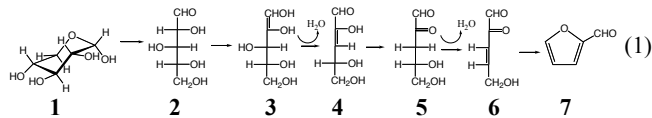
<sup>1</sup>National Bioenergy Center  
National Renewable Energy Laboratory  
Golden, Colorado 80401

## Introduction

The treatment of biomass with hot acid is an intriguing option for preparing cellulose for enzymatic hydrolysis or for directly hydrolyzing cellulose. The goal of these two procedures is to convert the cellulose in biomass into sugars that can either be used as a fermentation substrate for ethanol, a transportation fuel, or as a feedstock for chemical production. A key issue during hydrolysis is the yield of the sugars. Ideally one would like to convert all of the hemicellulose and cellulose to monosaccharides. However, it is known that some of the sugars formed by hydrolysis are decomposed under acidic conditions<sup>1</sup>. Further, it has been demonstrated that furanyl compounds are formed by this decomposition and these furanyl compounds can polymerize<sup>2</sup> and may restrict access to unreacted polysaccharides.

In spite of the importance of sugar decomposition in hot acid, there is uncertainty concerning the mechanisms of these processes. Reaction (1) shows a proposed mechanism<sup>2</sup> for conversion of xylose (**1**) to furfural (**7**) that involves a ring opening. Since xylan is an important constituent of corn stover, this process may be important in the full utilization of corn.

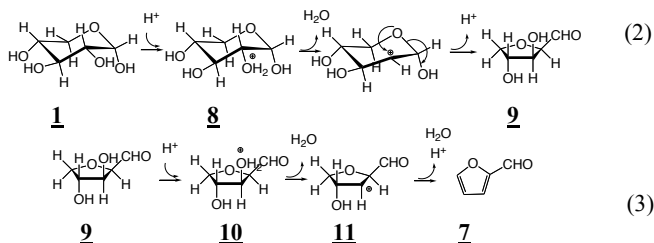
### Ring Opening Mechanism:



In this mechanism, the sugar in the pyran form opens to the aldehyde (**2**), which then tautomerizes to an enol (**3**). Dehydration of this enol by a six centered transition state to form **4**. Another tautomerization produces **5**, which dehydrates again to form **6**. This compound can cyclize and dehydrate to form furfural, **7**.

An alternative mechanism for forming furfural from xylose involves direct formation of the furan after protonation of the pyran<sup>3</sup> form (**1**). Xylose protonated at the 2 hydroxyl group can lose a water molecule and the resulting carbo cation is susceptible to attack by the ring ether forming a dihydroxy furan (**9**). This compound can then dehydrate to form furfural, **7**.

### Direct Mechanism:



We have studied the mechanisms of sugar decomposition shown in Rxns. (1) – (3) with quantum mechanical molecular modeling in an

attempt to determine which mechanism is prevalent. Small molecular systems are used to model the reaction steps shown in this mechanism. This allows the use of accurate computational techniques to capture the essential chemistry of these mechanisms.

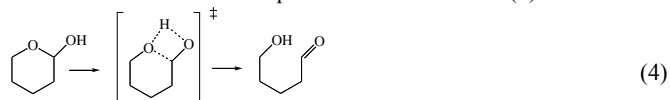
## Computational Techniques

The calculations in this study were carried out using the Gaussian 03 suite of programs. Local minima and transition states were found using Bery optimizations. Starting geometries for the transition state optimizations were often located using a potential energy scan, where one internal coordinate was systematically changed while all other coordinates were allowed to relax. The geometry at the calculated maximum of this scan was used as a starting geometry for a transition state (TS) optimization. Stable structures had only positive vibrational frequencies while transition states had one imaginary frequency. The transition states were confirmed by visual inspection of the imaginary frequency using the Molden visualization package.

## Results and Discussion

### Ring Opening Mechanism

The first step in this mechanism is the opening of the pyran ring, **1**, to form the aldehyde, **2**. This step involves a four-centered transition state as is shown for the simplified structure in Rxn. (4).



We have calculated the barrier for this reaction for several C5 and C4 sugars as well as hydroxymethyl methyl ether using density functional theory, B3LYP/6-31G(d). Values of 35 to 40 kcal mol<sup>-1</sup> were obtained. Figure 1 shows a plot of the calculated results for hydroxymethyl methyl ether. The barriers for these reactions are greatly reduced with the addition of proton. For instance, with hydroxymethyl methyl ether the barrier is lowered from 40.4 kcal mol<sup>-1</sup> to 14.3 kcal mol<sup>-1</sup> with the addition of a proton. This suggests that protic solvents or added acid should accelerate this rate. This lower barrier is also consistent with kinetic measurements made in water<sup>4</sup>.

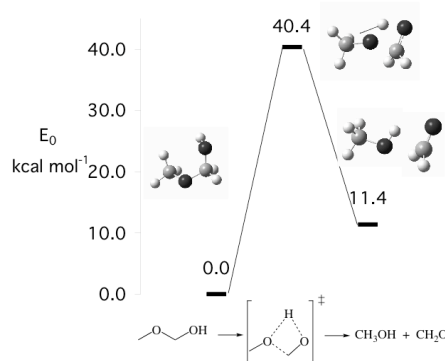
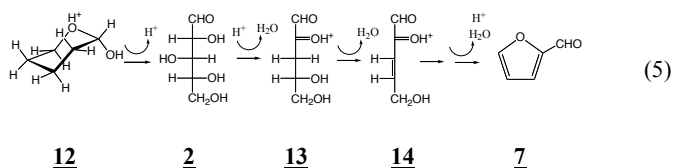


**Figure 1.** A potential energy plot of the calculated relative energies for the unimolecular decomposition of hydroxymethyl methyl ether.

The second step in the ring opening mechanism as shown in Rxn. (1) is a keto-enol tautomerization. Unfortunately, the barriers for these reactions are typically high. Our calculations show that the tautomerization of acetaldehyde to vinyl alcohol has a barrier of 67.8 kcal mol<sup>-1</sup>. We find that protonation does not significantly lower this barrier. Since the mechanism in Rxn. (1) contains two tautomerization steps, this pathway appears unlikely at practical temperatures.

We propose an alternative mechanism for furfural formation whereby the opened sugar undergoes a double dehydration as shown in reaction (5). In this mechanism, a proton catalyzes the ring opening step. Protonation of the C3 hydroxyl group on the resulting sugar, **2**, can lead to a double dehydration, forming **14**. This compound can then cyclize and further dehydrate to give furfural, **7**.



We have modeled this double dehydration using protonated glycerol as a model system. Figure 2 shows a plot of the calculated potential energy for this reaction. The barrier to loss of the first water molecule from protonated glycerol is 22.4 kcal mol<sup>-1</sup>. The barrier to the loss of a second water is calculated to be 36.5 kcal mol<sup>-1</sup>. This second barrier is high because a primary carbocation is formed. In double dehydration of xylose, Rxn. (5), a secondary carbocation is formed. We calculated the second barrier when a methyl group is attached to glycerol to better simulate dehydration in xylose. In this case the barrier is 21.7 kcal mol<sup>-1</sup> as shown in the figure. Thus the barriers for this double dehydration (22.4 and 21.7 kcal mol<sup>-1</sup>) are low enough that this reaction could be fast at moderate temperatures.

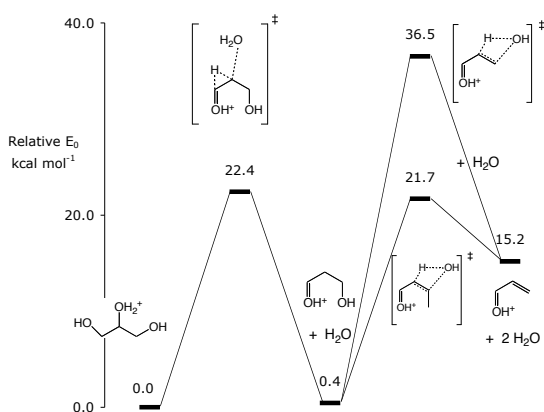


**Figure 2.** A potential energy plot of the calculated energies for the double dehydration of glycerol (CBS-QB3).

#### Direct Mechanism

We have calculated the barrier for a model reaction similar to reaction (2). The potential energy for the reaction of a protonated dihydroxy pyran is shown in Figure 3. We find that there is a concerted reaction for loss of water and rearrangement to the furan. The calculated barrier for this reaction is 13 kcal mol<sup>-1</sup>.

#### Calculated Rate Constants

The geometries and vibrational frequencies from these calculations can be used to estimate rate constants for the xylose decomposition reactions. These calculated values are used to estimate the entropy change in going from a reactant to a transition state ( $DS^\ddagger$ ), which is used to calculate the pre-exponential Arrhenius factor using Transition State Theory (TST).

$$A_{TST} = \left( \frac{kt}{h} \right) \left( \frac{1}{RT} \right)^{\Delta n} e^{(\ddagger - \Delta n)} \exp(\Delta S^\ddagger / RT) \quad (6)$$

Rate constants calculated using Eqn. 6 are collected in Table 1. As can be seen, the rate constants are high at typical pretreatment

conditions. The activation energies,  $A_{TST}$ , for these mechanisms are consistent with measure global activation energies for xylose decomposition<sup>5</sup>. The table is divided into rate constants for the ring opening mechanism, left, and the direct mechanism, right.

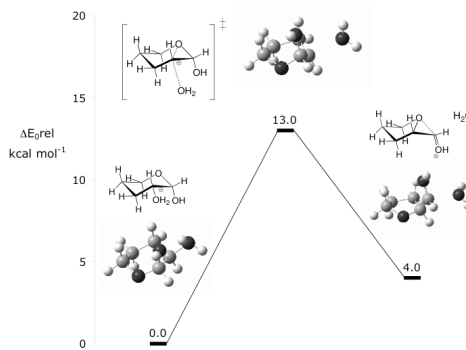


**Figure 3.** Plot of the potential energy for the direct conversion of a protonated pyran to a furan.

**Table 1** Calculated rate constants using TST

	Ring Opening Mech.			Direct
	Ring Opening	1 <sup>st</sup> Dehyd.	2 <sup>nd</sup> Dehyd.	Rxn 2
Ea (kcal mol <sup>-1</sup> )	14.3	20.9	21.7	13.0
$A_{TST}$ (s <sup>-1</sup> )	$8.2 \times 10^{13}$	$6.3 \times 10^{14}$	$6.3 \times 10^{14}$	$6.3 \times 10^{14}$
Temp. (°C)	Calculated TST Rate Constants			
100	$3.4 \times 10^5$	$9.1 \times 10^3$	$4.6 \times 10^2$	$1.5 \times 10^7$
150	$3.3 \times 10^6$	$2.5 \times 10^5$	$1.5 \times 10^2$	$1.2 \times 10^8$
200	$2.0 \times 10^7$	$3.5 \times 10^6$	$2.2 \times 10^5$	$6.2 \times 10^8$

#### Conclusions

The rate constants that we obtain for the ring opening mechanism appear to be lower than for the direct mechanism. However, this does not include the dehydration steps such as are shown in Rxn. (3). These reactions should have barriers of about 20 kcal mol<sup>-1</sup>, which should make the two mechanisms more comparable.

#### Acknowledgment

We would like to acknowledge The Office of the Biomass Program of the U.S. Department of Energy, who funded portions of this work and the National Center for Supercomputer Applications (NCSA Grant # CHE-980028n) for computer time.

#### References

- van Dam, H. E.; Kieboom, A. P. G.; van Bekkum, H. *Starch* **1986**, 38, 95.
- Kuster, B. F. M. *Starch*, **1990** 42, 314
- Antal, M. J., Jr.; Leesomboon, T.; Mok, W. S.; Richards, G. N. *Carbohydrate Res.* **1991**, 217, 71.
- Serianni, A. S.; Pierce, J.; Huang, S-G.; Barker, R. *J. Am. Chem. Soc.* **1982**, 104, 4037.
- McKibbins, S. W.; Harris, J. F.; Saeman, J. F. *Forest Prod. J.* **1962**, 17.; van Dam, H. E.; Kieboom, A. P. G.; van Bekkum, H. *Starch*, **1986**, 38, 95

# MECHANISTIC INVESTIGATION INTO THE FORMATION OF POLYCYCLIC AROMATIC HYDROCARBONS FROM THE PYROLYSIS OF TERPENES

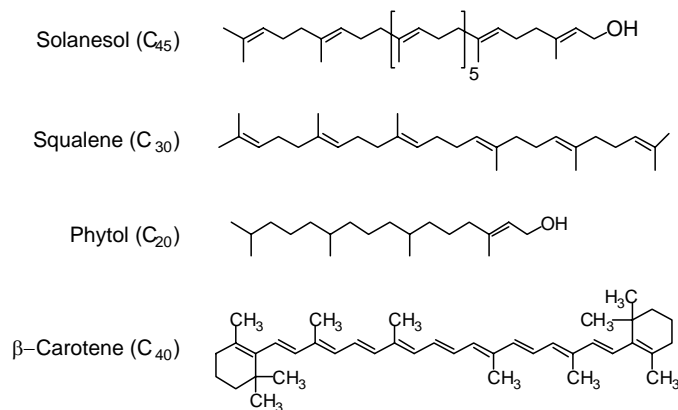
Phillip F. Britt, A. C. Buchanan, III, and Clyde V. Owens, Jr.

Chemical Sciences Division  
Oak Ridge National Laboratory  
P.O. Box 2008, Oak Ridge, TN 37831-6197

## Introduction

Currently, there is interest in utilizing renewable energy resources, such as wood and agriculture waste, for power generation, production of liquid fuels, and specialty chemicals as a consequence of the environmental benefits.<sup>1</sup> However, pyrolysis, gasification, and combustion of biomass produces polycyclic aromatic hydrocarbons (PAHs), which are environmental pollutants and soot precursors.<sup>2,3,4,5,6,7</sup> In pyrolysis, PAHs are proposed to be formed by pyrosynthesis, in which radicals undergo a series of bimolecular reactions with alkenes, alkynes, and aromatics to form larger ring structures. The yield of PAHs are found to increase with temperature and gas phase residence times.<sup>8,9</sup> In gasification and combustion, it has been postulated that PAHs arise from pyrolysis reactions in oxygen-deficient regions.<sup>10</sup> A better fundamental understanding of the initial pyrolysis reactions that occur in the thermochemical processing of biomass, and subsequent reactions of the vapor phase products could provide insight into reducing PAH emissions from biomass combustion, reducing tar formation from gasification, and enhancing production of specialty chemicals from the fast pyrolysis of biomass.

As a consequence of the chemical complexity of biomass and its pyrolysis products, it has been difficult to gain detailed information on the formation pathways of specific products.<sup>11,12</sup> Thus, to gain fundamental kinetic and mechanistic information on product formation in biomass pyrolysis, efforts have focused on the pyrolysis of key chemical constituents found in biomass. In our previous investigations, we have focused on the pyrolysis of plant steroids as potential precursors to PAHs.<sup>13,14</sup> It was shown that the native ring structure of the steroid was maintained to form PAHs, such as phenanthrene and chrysene, and the yield of PAHs was dependent on the steroid structure. PAH yield and ring size were also shown to increase with residence time, temperature, and concentration. In this investigation, the pyrolysis of plant terpenes was investigated at 600–800 °C and at short residence times ( $\leq 1$  s). This study focused on the pyrolysis of solanesol, squalene, phytol, and  $\beta$ -carotene. These terpenes are



predominately found in the foliage. The yield of PAHs from the pyrolysis of terpenes will be compared to those found from steroids to determine if the alkenes produced from the pyrolysis of terpenes, such as isoprene, enhance the formation of PAHs.

## Experimental

The flow pyrolysis reactor used in this study has been previously described.<sup>7</sup> After the pyrolysis, both cold traps were washed with CS<sub>2</sub>, and the washings were combined (total volume 10–20 mL). Solutions of hexatriacontane, phenanthrene-*d*<sub>10</sub>, and 1,2-benzanthracene-*d*<sub>12</sub> were added as standards, and the reaction mixtures were analyzed by GC-MS and quantitated by GC-FID as previously described. Typical shot to shot reproducibility was  $\pm 2\%$  with the exception of the smaller products ( $< 0.1$  mol%) in the presence of a large background in which the shot to shot reproducibility was typically  $\pm 5$ –10%. Products were quantitated by averaging the GC-FID output relative to the internal standards. Response factors were measured with authentic samples or estimated from measured response factors for structurally related compounds and based on carbon number relative to the internal standards (hexatriacontane, phenanthrene-*d*<sub>10</sub> or 1,2-benzanthracene-*d*<sub>12</sub>). The limits of detection (LOD) for the PAHs depended upon the complexity of the reaction mixture, but the LOD was typically 5–20  $\mu\text{g g}^{-1}$ .

The residence time in the reaction chamber was calculated from the volume of the reactor (1.06 mL or 11.7 mL) in the hot zone, the helium flow rate at room temperature, and a correction for the gas flow rate at the reaction temperature. The reactor was also calibrated by the pyrolysis of phenethyl acetate, whose well-defined first order kinetics allows verification of the reactor temperature and residence time.

## Results and Discussion

The flow pyrolysis of solanesol was investigated at high concentration at 700 and 800 °C with residence times of 0.13 and 1.0 s. The yields of selected PAHs are shown in Table 1. One surprising observation was the lack of substantial quantities of 3-ringed or larger PAHs at temperatures less than 800 °C. On the basis of Severson's study,<sup>15</sup> it was expected that solanesol would produce significant quantities of PAHs, since it was concluded that solanesol contributed as much as 40% of the benzopyrenes produced from the pyrolysis of the petroleum ether extract of tobacco. Duplicate pyrolysis runs at 800 °C produced product yields that were  $\pm 20$ –30% of those reported in Table 1 confirming the low yields of PAHs from the pyrolysis of solanesol.

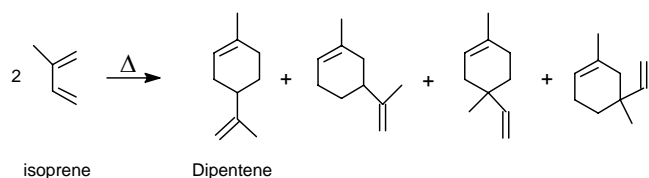
At 600 °C and 0.13 s residence time, dipentene (limonene, *m/z* 136) and isoprene (*m/z* 68) were the dominant products. Small amounts of toluene, *m*-xylene and isomeric products with *m/z* 136 (4 isomers) and 138 (1-methyl-4-(1-methylethyl)cyclohexene and isomer) were also found. At 700 °C with 0.13 s residence time, *m*-xylene, toluene, and isoprene were the dominant products, and only small amounts of dipentene and isomers were found. Small amounts of aromatic products, such as trimethylbenzene, methylisopropenylbenzene, methylindene, and methyl-naphthalene, were also formed. A similar product distribution was found in the low concentration (68 mg h<sup>-1</sup>, 3 $\times 10^{-6}$  M), short residence time (0.15 s), flow pyrolysis of solanesol at 700 °C, but the product yields were lower. As the temperature and residence times increased, larger PAHs, such as phenanthrene, were detected. However, four ringed aromatic compounds, such as pyrene and chrysene, were only found at 800 °C. Increasing the residence time from 1.0 s to 9.0 s at 700 °C significantly increased the yield of PAHs. It appears that solanesol only forms significant quantities of 3–5 ringed aromatics at high temperatures (800 °C) or at long residence times ( $\geq 1$  sec).

**Table 1. Product Yields From the Flow Pyrolysis of Solanesol at High Concentration.**

Temperature (°C)	700	700	700	700	800
Contact Time (s)	0.13	0.15	1.0	9.0	1.0
Concentration (μM) <sup>a</sup>	130	3.0	83	130	72
Products (mg/g)					
Benzene	8.50	4.6	23.1	ND	67.6
Toluene	30.2	22.7	47.8	ND	61.3
Styrene	6.70	5.4	12.6	ND	21.5
Indene	2.03	0.16	5.45	ND	12.6
Naphthalene	0.91	0.53	3.67	ND	23.2
2-Methylnaphthalene	1.72	0.91	4.40	ND	13.4
1-Methylnaphthalene	1.07	0.55	2.94	10.8	8.28
Acenaphthylene	0.51	0.00	1.28	2.2	6.47
Fluorene	0.00	0.00	0.77	ND	2.97
Phenanthrene (Phen)	0.00	0.00	0.37	2.7	4.10
Anthracene (An)	0.00	0.00	0.26	0.88	1.90
MethylPhen/An	0.00	0.00	1.30	5.4	6.71
Fluoranthene	0.00	0.00	0.00	0.89	0.71
Pyrene	0.00	0.00	0.00	1.5	1.15
Methylpyrenes	0.00	0.00	0.00	3.5	3.84
Benz[ <i>a</i> ]anthracene	0.00	0.00	0.00	0.42	0.67
Chrysene	0.00	0.00	0.00	0.38	0.61
Benzo[ <i>a</i> ]pyrene	0.00	0.00	0.00	0.42	0.39

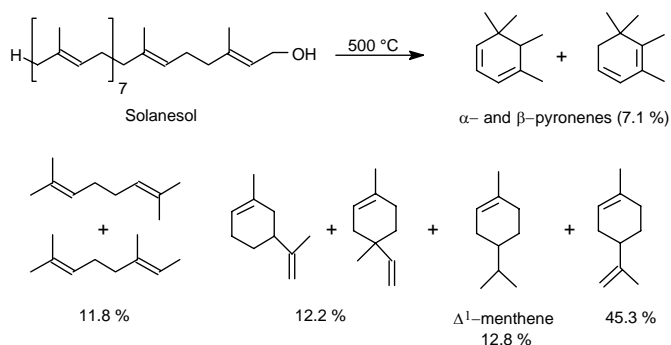
<sup>a</sup> Concentration determined by sublimation rate/gas flow rate at the reaction temperature. ND = Not Determined.

It had been previously proposed that the terpene components of tobacco form PAHs by decomposing into isoprene and pyrosynthesis into larger PAHs.<sup>16</sup> Isoprene is the major component of the unsaturated gaseous hydrocarbons present in tobacco smoke<sup>17</sup> and pyrolysis of isoprene at 600–800 °C forms PAHs, including benzo[*a*]pyrene (2-3 s residence time).<sup>18</sup> Larger PAHs can form from isoprene pyrolysis by concerted Diels–Alder or free radical reactions. Dimerization of isoprene, via Diels–Alder reaction, yields dipentene (also called *p*-mentha-1,8-diene or limonene) and mixtures of dimethylvinylcyclohexenes (see below), but tobacco smoke contains only dipentene and 2,4-dimethyl-4-vinylcyclohexene.<sup>19</sup>

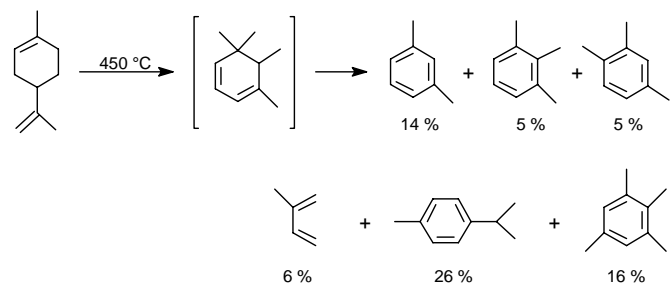


This suggests that free radical pathways form the products in tobacco. The pyrolysis of solanesol has been studied previously (residence time unknown), and it was found that at temperatures up to 550 °C, the hydrocarbon fraction was mainly composed of monoterpenoids with only traces of aromatic hydrocarbons.<sup>20</sup> For example, pyrolysis of solanesol at 500 °C under nitrogen produced pyrenenes, dimethyloctadiene, dimethylvinylcyclohexenes,  $\Delta^1$ -menthene, and dipentene. The major gas phase products were isoprene (64 parts), 2-methyl-2-butene (8 parts), and one part each of 2-methyl-1-butene and 3-methyl-1-butene. Running the pyrolysis in hydrogen altered the product yields confirming that the products were formed by free radical rather than a concerted pathway. At 600 °C, the monocyclic fraction (93 % by weight of the total sample) contained benzene (5 wt%), toluene (30 wt%), xylenes (38 wt%) and

$C_9$  alkylbenzenes (21 wt%). Similar results were found in our study at 600 °C. At temperatures above 650 °C, only aromatic compounds were formed and no terpenes were found.



The pyrolysis of dipentene (limonene) has been studied at 450 °C over copper pellets (residence time unknown).<sup>21</sup> The dominant products were pyrenenes, other alkylcyclohexadienes, and a small amount (9%) of aromatic hydrocarbons. It was proposed that limonene decomposed by a biradical mechanism in which radicals from C–C homolysis of the bisallylic bond underwent disproportionation to form a triene that can isomerize (1,5-hydrogen shift) and undergo electrocyclic ring closure to form the pyrenenes and 1,3-dimethyl-1-ethyl-3,5-cyclohexadiene (not shown). Independent pyrolysis of the pyrenenes at 450 °C gave a similar distribution of aromatic hydrocarbons.



Thus, on the basis of the literature evidence, it is proposed that solanesol decomposes directly to isoprene and dipentene, as the major products, and alkylcyclohexenes by a free radical pathway. Depending on the reaction severity (residence time and temperature), these initial products can undergo additional free radical reactions to form alkyl-substituted monocyclic aromatic hydrocarbons, and larger PAHs. A potential mechanism for dipentene formation by a free radical pathway is shown in Figure 1a. The TG-MS of solanesol showed a significant loss of water at relatively low temperatures (i.e., 360 °C). Therefore, water can be eliminated by a concerted 1,4-elimination to form a terminal diene. Homolysis of the bisallylic C–C bond forms an isopropenyl radical ( $C_5H_7\cdot$ ) that can hydrogen abstract from solanesol to give isoprene. The allylic radical can undergo an intramolecular 1,6-cyclization reaction competitively with  $\beta$ -scission. As previously reported, the ratio of intramolecular radical addition to  $\beta$ -scission for 1-hex-5-enyl radical is 124 at 650 °C and 39 at 750 °C, which indicates that cyclization should dominate.<sup>22</sup> After cyclization,  $\beta$ -scission of the tertiary radical forms dipentene and a radical that can continue the

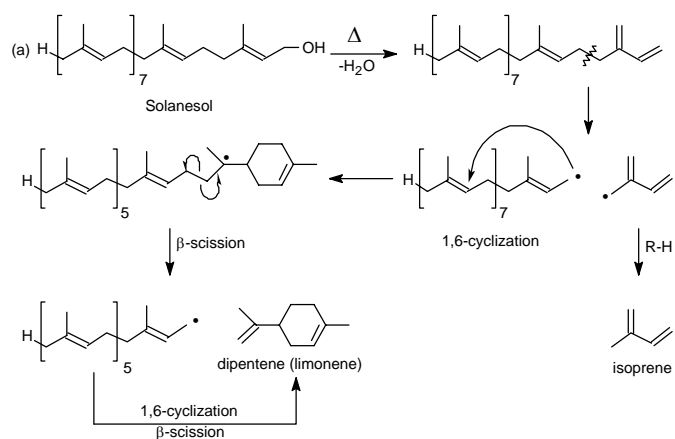


**Figure 1a.** Mechanism for the formation of dipentene and isoprene from solanesol.

unzipping process. Hydrogen abstraction from solanesol at the allylic site between the double bonds also forms an intermediate that can undergo 1,6-cyclization to form dipentene. Hydrogen abstraction from the methyl group (Figure 1b) followed by 1,6-cyclizations and  $\beta$ -scission forms 2,4-dimethyl-4-vinylcyclohexene (which is found in tobacco smoke).

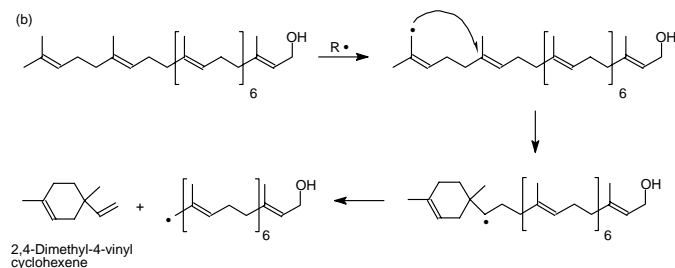


**Figure 1b.** Formation of 2,4-dimethyl-4-vinylcyclohexene from the decomposition of solanesol.

Larger PAHs must arise from reaction of the monocyclic aromatic hydrocarbons with the low molecular weight unsaturated products, such as isoprene. In the combustion of 1,3-butadiene in a sooting flame (i.e., fuel rich flame), it was concluded that monocyclic PAHs were made by free radical pathways involving  $C_4H_5\cdot$  as the dominant species. The Diels-Alder reaction of butadiene was too slow and concentration of the reagents too low, to account for the PAHs formed in the flame.<sup>23</sup> In the pyrolysis of solanesol, larger PAHs are most likely formed by a similar pathway with aromatic and benzylic radicals adding to unsaturated products, such as isoprene, in the hot zone of the furnace (i.e., pyrosynthesis). However, the specific reaction pathway from the primary products (i.e., isoprene and dipentene) to the large PAHs are only implied and are not specifically known. Solanesol and other terpenes could also enhance PAH yields from pyrolysis of other substrates by providing hydrocarbons (i.e., isoprene) for pyrosynthesis. For example, in the pyrolysis of cellulose, replacing the nitrogen carrier gas with propene increased the yield of benzo[a]pyrene 1.9 fold at 350-450 °C and 6.9 fold at 450-550 °C even though the propene did not produce benzo[a]pyrene at temperatures >550 °C.<sup>24</sup>

Preliminary results on the yield of PAHs produced from the pyrolysis of solanesol,  $\beta$ -carotene, squalene, and stigmasterol (a plant steroid) at 800 °C with a residence time of 1.0 s is shown in

Figure 2. In general, the steroid produces more PAHs than the terpenes, especially phenanthrene, anthracene, benz[a]anthracene, and chrysene which can be derived from dehydrogenation, dealkylation, and rearrangement of the steroid. Surprisingly, squalene produces fewer PAHs than solanesol. The pyrolysis of  $\beta$ -carotene and squalene is currently being investigated at 700 and 600 °C with a residence time of 1.0 s and 0.13 s. These results will be discussed in the oral presentation.

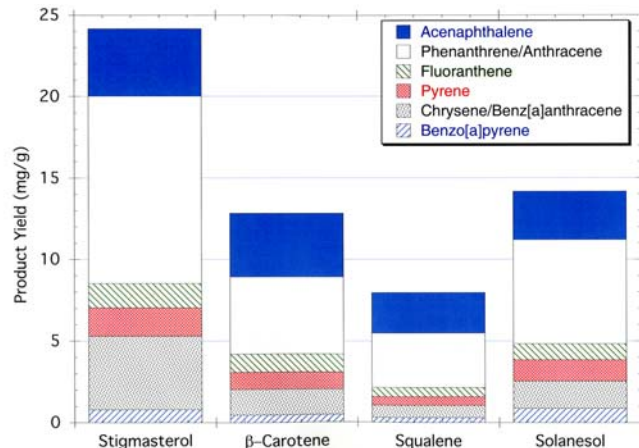


**Figure 2.** PAH yields from the pyrolysis of terpenes at 800 °C in helium with a residence time of 1.0 s.

## Conclusions

In this investigation, terpenes were found to produce three, four, and five-membered aromatic hydrocarbons at high temperatures and at short residence times. At long residence times, the yield of larger PAHs, such as benz[a]anthracene and benzo[a]pyrene, increase more than the yield of smaller PAHs, such as phenanthrene and fluoranthene. Although terpenes produce fewer PAHs than steroids (stigmasterol), terpenes produce large yields of low molecular weight products such as isoprene, toluene and xylenes. Under short residence time conditions, it does not appear that the low molecular weight hydrocarbons enhance the pyrosynthesis of PAHs.

**Acknowledgement.** This research was supported by Philip Morris USA. Additional support was provided by the Division of Chemical Sciences, Geosciences and Biosciences, Office of Basic Energy Sciences, U.S. Department of Energy, under contract DE-AC05-00OR22725 with Oak Ridge National Laboratory, managed and operated by UT-Battelle, LLC. CVO was supported by an appointment to ORNL Postdoctoral Research Program administered jointly by Oak Ridge Institute for Science and Education and ORNL.

## References

- (1) *Developments in Thermochemical Biomass Conversion*; Bridgwater, A. V., Boocock, D. G. B., Eds.; London: Blackie Academic, 1997 and references therein.
- (2) Mastral, A. M.; Callén, M. S. *Environ. Sci. Technol.* **2000**, *34*, 3051.
- (3) Elliott, D. C. In *Pyrolysis Oils From Biomass*; Doltes, E. J., Milne, T. A., Eds.; ACS Symposium Series 376, Washington, DC: American Chemical Society, 1988, pp 55.
- (4) *Fundamentals of Thermochemical Biomass Conversion*; Overend, R. P.; Milne, T. A.; Mudge, L. K., Eds.; London: Elsevier Applied Science, 1985 and references therein.
- (5) Khalfi, A.; Trouvé, G.; Delobel, R.; Delfosse, L. *J. Anal. Appl. Pyrolysis* **2000**, *56*, 243.
- (6) Brage, C.; Yu, Q.; Sjöström, K. *Fuel* **1996**, *75*, 213.
- (7) Homann, K. -H. *Angew. Chem. Int. Ed.* **1998**, *37*, 2434.

- 
- (8) Richter, H.; Howard, J. B. *Prog. Energy Combust. Sci.* **2000**, *26*, 565 and references therein.
- (9) Marinov, N. M.; Pitz, W. J.; Westbrook, C. K.; Vincitore, A. M.; Castaldi, M. J.; Senkan, S. M.; Melius, C. F. *Combust. Flame* **1998**, *114*, 192.
- (10) Marsh, N. D.; Zhu, D.; Wornat, M. J. *Proceedings of the Combustion Institute* **1998**, *27*, 1897.
- (11) Antal, M. J., Jr. In *Biomass Pyrolysis: A Review of the Literature Part II-Lignocellulose Pyrolysis.*; Beor, K. W.; Duffie, J. A., Eds.; Advances in Solar Energy, New York; ASES Publications; 1982, p. 61 and references therein.
- (12) Antal, M. J., Jr. In *Biomass Pyrolysis: A Review of the Literature Part I-Carbohydrate Pyrolysis.*; Beor, K. W., Duffie, J. A., Eds.; Advances in Solar Energy, New York; ASES Publications; 1985; p. 175 and references therein.
- (13) Britt, P. F.; Buchanan, A. C., III; Kidder, M. K.; Owens, C.; Ammann, J. R.; Skeen, J. T.; Luo, L. *Fuel* **2001**, *80*, 1727.
- (14) Britt, P. F.; Buchanan, A. C., III; Kidder, M. K.; Owens, C. V., Jr. *J. Anal. Appl. Pyrolysis* **2003**, *66*, 71.
- (15) Severson R. F.; Schlotzhauer, W. S.; Chortyk, O. T.; Arrendale, R. F.; Snook, M. E. In *Polynuclear Aromatic Hydrocarbons*; Jones, P. W., Leber P. Eds.; Ann Arbor, MI Ann Arbor Science, 1979, p 277.
- (16) Gil-Av E.; Shabtai, J. *Nature* **1963**, *197*, 1065.
- (17) Vilcins, G. *Beitr. Tabakforschung* **1975**, *8*, 181.
- (18) Oró, J.; Han, J.; Zlatkis, A. *Anal. Chem.* **1967**, *39*, 27.
- (19) Stedman R. L. *Chem. Rev.* **1968**, *68*,153.
- (20) Grossman, J. D.; Ikeda, R. M.; Deszyck, E. J.; Bavley, A. *Nature* **1963**, *199*, 661.
- (21) Pines, H.; Ryer, J. *J. Am. Chem. Soc.* **1955**, *77*, 4370.
- (22) (a) Handford-Styring, S. M.; Walker, R. W. *J. Chem. Soc., Faraday Trans.* **1995**, *91*, 1431. The rate expression for  $\beta$ -scission to form ethylene and 1-but-3-enyl radical is  $\log k(\text{s}^{-1}) = 13.0 - 29.9/\theta$ , while intramolecular cyclization has a rate expression of  $\log k(\text{s}^{-1}) = 10.0 - 8.4/\theta$ . (b) For a cyclic system, the rate expression for the intramolecular cyclization of the 2-allylbenzyl radical is  $\log k(\text{s}^{-1}) = 11.14 - 16.28/\theta$ .
- (23) Cole, J. A.; Bittner, J. D.; Longwell, J. P.; Howard, J. B. *Combust. Flame* **1984**, *56*, 51.
- (24) Robb, E. W.; Johnson, W. R.; Westbrook, J. J.; Seligman, R. B. *Beitr. Tabakforschung* **1966**, *3*, 597.